Available online at www.sciencedirect.com

ScienceDirect

Solar Energy 131 (2016) 275–295

SOLAR ENERGY

www.elsevier.com/locate/solener

Experimental and CFD investigation of convection heat transfer in solar air heater with reverse L-shaped ribs

Vipin B. Gawande [a,*], A.S. Dhoble [a], D.B. Zodpe [a], Sunil Chamoli [b]

[a] *Department of Mechanical Engineering, Visvesvaraya National Institute of Technology, Nagpur, India*
[b] *Department of Mechanical Engineering, D.I.T University Dehradun, India*

Received 7 January 2015; received in revised form 10 December 2015; accepted 20 February 2016

Communicated by: Associate Editor D. Yogi Goswami

Abstract

A solar air heater is a thermal system which uses artificial roughness in the form of repeated ribs on the absorber plate to enhance the heat transfer rate. Forced convection heat transfer of air in a solar air heater with reverse L-shaped ribs has been carried out experimentally and numerically. Thermal performance of solar air heater is studied with design variables such as relative roughness pitch ($7.14 \leqslant P/e \leqslant 17.86$), Reynolds number ($3800 \leqslant Re \leqslant 18{,}000$), heat flux ($1000\ \mathrm{W/m^2}$) and constant relative roughness height ($e/D = 0.042$). A two dimensional CFD simulation is carried out with using CFD code, ANSYS FLUENT and RNG k–ε turbulence model, for solving turbulence terms in governing equations. The presence of reverse L-shaped rib shows a significant effect on heat transfer and friction factor characteristics, relative to change in relative roughness pitch (P/e) and Reynolds number (Re). Thermo hydraulic performance parameter (T.H.P.P) of 1.90 considering heat transfer augmentation with same pumping power, has been evaluated for optimum configuration of the roughness element (reverse L-shaped rib) for artificially roughened solar air heater. It has been found that the numerical results are in good agreement with the experimental results for the range of parameters investigated. Correlations for Nusselt number and friction factor have been developed as a function of roughness and flow parameters.

Keywords: Solar air heater; Reverse L-shaped rib; Artificial roughness; Friction factor; Heat transfer; CFD

1. Introduction

In our nature, we have abundant amount of solar energy, which may be extensively used as an energy source. So among research community in the world, solar energy utilization for society has become one of the most important issues. Solar air heater is one among solar thermal systems which is extensively used for heating purposes like drying of crops, space heating, winter home heating, seasoning of timber, etc. In rectangular solar air heater duct, heat is transferred from the heated wall (top surface of duct) comprising the absorber plate to incoming air and the other walls are kept insulated. In solar air heater, the heat transfer coefficient between heated absorber plate and working medium, air, is poor which leads to lower efficiency of the solar air heater. The efficiency of the solar air heater increases when the artificial roughness is provided on the absorber plate. Artificial roughness thus provided penetrates the viscous sub layer which increases the intensity of turbulence in the duct and causes enhancement in heat transfer from the roughened surface as compared to smooth surface. The arrangement also increases friction

* Corresponding author. Tel.: + 91 9890659696.
E-mail address: vipingawande@gmail.com (V.B. Gawande).

http://dx.doi.org/10.1016/j.solener.2016.02.040
0038-092X/

Nomenclature

D	equivalent or hydraulic diameter of duct, mm
e	rib height
h	heat transfer coefficient
H	depth of the duct
k	thermal conductivity of air, W/mK
L_1	inlet length of duct, mm
L_2	test length of the duct, mm
L_3	outlet length of duct, mm
P	pitch, mm
T	air temperature, K
U	mean air flow velocity in the duct, m/s
u	air flow velocity in x-direction, m/s
v	air flow velocity in y-direction, m/s
W	width of the duct
ΔP	pressure drop, Pa

Dimensionless parameters

e/D	relative roughness height, mm
f	friction factor
f_r	friction factor for rough surface
f_s	friction factor for smooth surface
Nu	Nusselt number
Nu_r	Nusselt number for rough surface
Nu_s	Nusselt number for smooth surface
Pr	Prandtl number
P/e	relative roughness pitch
Re	Reynolds number
W/H	duct aspect ratio

Greek symbols

μ	dynamic viscosity, Ns/m^2
μ_t	turbulent viscosity, Ns/m^2
ρ	density of air, Ns/m^2
Γ	molecular thermal diffusivity
Γ_t	turbulent thermal diffusivity
β	ratio of orifice diameter to pipe diameter
ε	dissipation rate

in the duct which in turn increases pumping power requirements for air through the duct.

In the research area of solar air heater, many researchers have proposed various artificial roughness geometries for the enhancement of heat transfer rate. In the literature given in this paper, various designs suggested by researchers are discussed. Prasad and Mullick (1983) experimentally investigated the effect of small diameter wire attached on the underside of the absorber plate as a artificial roughness. Small diameter protrusion wires are also used for the different operating and geometrical parameters by Prasad and Saini (1988) and Kays (1966). Experimental investigation of Gupta et al. (1993) reported that staton number increases initially up to Reynolds number of 12,000 and then decreases for further increase in Reynolds number by providing transverse wire as artificial roughness on absorber plate in solar air heater duct. Experimental investigation was carried out by Sahu and Bhagoria (2005) using 90° broken transverse broken ribs oh heat and fluid flow characteristics in solar air heater. Experimental studies were carried out by Han and Park (1989) using inclined ribs in narrow aspect ratio ducts which show considerable increase in heat transfer enhancement. Gupta et al. (1997) studied the effect of inclination of rib with respect to flow direction for transitionally rough flow region. Aharwal et al. (2008) have investigated the effect of width and position of gap in inclined split ribs having square cross sections on heat transfer and friction characteristics of rectangular solar air heater duct. Kumar et al. (2011) have developed statistical correlations for Nusselt number and friction factor as a function of gap position, rib height, pitch and Reynolds number using 60° inclined discrete ribs on absorber plate of solar air heater duct. The effect of combined inclined and transverse rib on heat transfer enhancement and flow characteristics has been investigated by Varun et al. (2008). Momin et al. (2002) have experimentally studied the effect of V-shaped roughness. Karwa (2003) has experimentally investigated the effect of transverse, inclined, V-up continuous and V-down continuous, V-up discrete ribs and V-down discrete ribs in a high aspect ratio duct. The effect of wedge shaped transverse repeated rib roughness on heat transfer and flow characteristics of solar air heater duct has been experimentally investigated by Bhagoria et al. (2002). Gupta and Kaushik (2009) have carried out parametric study of artificial roughness geometry in the form of expanded metal mesh type on the absorber plate of solar air heater duct. Bhushan and Singh (2011) have experimentally investigated the effect of protrusion as roughness on heat transfer and friction in solar air heater. Sethi et al. (2012) have experimentally investigated the effect on heat transfer and flow characteristics using dimple shaped elements arranged in angular fashion as roughness elements on the absorber plate of solar air heater duct. The effect of arc shape parallel wire as roughness element on the absorber plate to study thermo hydraulic performance of solar air heater have been investigated by Saini and Saini (2008). Karmare and Tikekar (2007) have experimentally investigated the effect of metal grit ribs on heat transfer and flow characteristics of solar air heater. Experimental investigations with W-shape ribs on absorber plate of solar air heater duct have been carried out by Lanjewar et al. (2011). The effect

Table 1
Thermo-hydraulic performance parameter (THPP) at relative roughness pitch (P/e) of 7.14 and $Re = 15{,}000$, for square rib investigated in literature.

S. No	Name of researcher	Roughness geometry	Thermo hydraulic performance parameter (T.H.P.P)
1	Yadav and Bhagoria (2013a)	Square sectioned transverse rib	1.78
2	Yadav and Bhagoria (2014a)	Square sectioned transverse rib	1.85

of discrete W-shaped ribs was experimentally studied by Kumar et al. (2008). The effect of inverted U shaped turbulators on heat transfer and friction characteristics of solar air heater duct have been experimentally studied by Bopche and Tandale (2009). Yeh and Chou (1991) have experimentally investigated the effect of baffles on thermo hydraulic performance of the solar air heater. The details of various roughness geometries used by the researchers are described and explained in the author's paper (Gawande et al., 2014a).

Along with experimental investigations, researchers have also carried out numerical analysis of solar air heater duct with artificial roughness on the absorber plate. The main advantage of using numerical analysis is that, it helps to predict the results before actual experimental installation. Today, the development of advanced numerical methodologies and high speed computation, allows researchers to carry out complex fluid flow simulations in a very short duration of time. Literature review in this area shows that very few researchers have carried out CFD investigations of artificially roughened solar air heater. The details review of CFD analysis carried out in solar air heater to evaluate the optimum rib shape and configuration which can enhance convective heat transfer with minimum pumping power is given in our recently published paper (Gawande et al., 2016a).

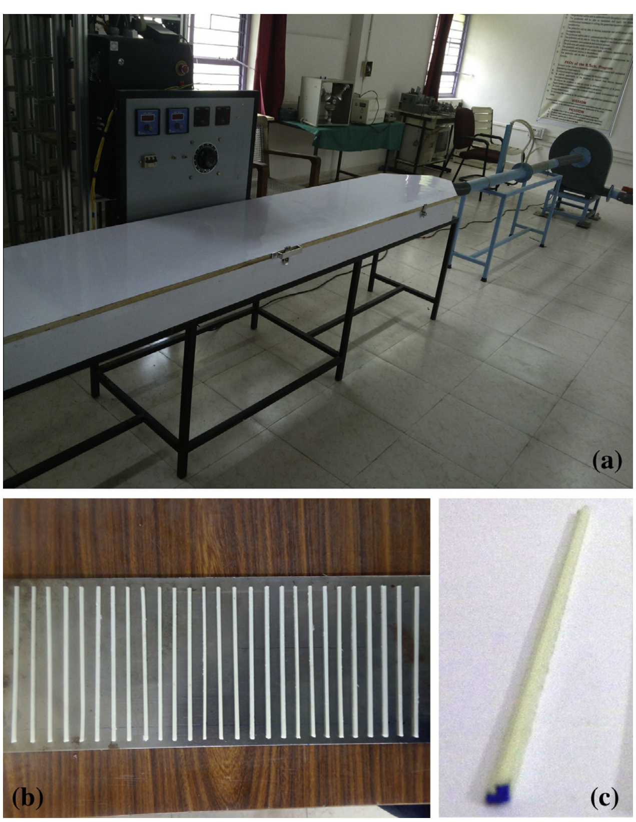

Fig. 1. (a) Pictorial view of experimental set up of solar air heater, (b) top view of test section with reverse L-shaped roughness and (c) individual L-shaped rib.

Though the insertion of artificial roughness on underside of absorber plate of solar air heater enhances the heat transfer rate, it also causes friction losses in the duct. So researchers always tried out to investigate the optimum configuration of rib to increase heat transfer in solar air heater duct with minimum pumping power. The variation of themo hydraulic performance parameter (THPP) with relative roughness pitch (P/e) of 7.14 and at $Re = 15{,}000$, for square rib is shown in Table 1. Table 1 shows that the value of THPP for square rib for $P/e = 7.14$ and at $Re = 15{,}000$. As observed from the numerical analysis of Yadav and Bhagoria (2013a,b, 2014a), decrease in relative roughness pitch (P/e) increases heat transfer rate in solar air heater. The shape of the rib cross section affects the formation of vortices behind the rib and increases amount of turbulent kinetic energy (see Figs. 13 and 14). Authors feel there is a scope to increase the thermo hydraulic performance of solar air heater by making slight modification in square rib roughness geometry. So a new kind of rib shape is designed to study the effect of relative roughness pitch (P/e) and Reynolds number on the flow characteristics in solar air heater duct. The present paper presents new roughness geometry in the form of reverse L-shaped rib and its effect on thermal performance of solar air heater which may be used for the enhancement of heat transfer in solar air heater. Comparison between the experimental and CFD results is also presented in this paper.

Finally, the objectives of the present analysis are:

(1) To investigate the effect of relative roughness pitch and Reynolds number on the heat transfer enhancement and flow friction characteristics using reverse L-shaped ribs artificial roughness mounted on the underside of the absorber plate of solar air heater by experimental and numerical (CFD) analysis.
(2) To find out the optimal configuration of reverse L-shaped rib roughness for the maximum heat transfer enhancement and minimum pumping power requirement in terms of thermo hydraulic performance param eter using both CFD and experimental investigation.

2. Experimental set up

The pictorial and schematic representation of experimental facility and test section with roughened ribs mounted on absorber plate of solar air heater duct is shown in Fig. 1 and Fig. 2 respectively. The main components of the experimental set up are a blower, wooden rectangular duct, electric heater, G.I pipe, control valves, orifice plate, U-tube manometer, Micro Manometer (MM), variable transformer, voltmeter, ammeter, thermocouples and mili-voltmeter. Air at room temperature enters a rectangular duct (width $W = 0.1$ m, height $H = 0.02$ m, aspect ratio $W/H = 5$, hydraulic diameter, $D = 0.033$ m) because of open circuit suction type high pressure blower. The rectangular duct consists of an entry section, test section (0.280 m) and exit section which was taken as per ASHRAE standards 93-77 (ASHRAE Standard 93, 2003). A 0.5 mm thick heater plate (0.1 m wide and 0.280 m long) was fabricated by combining series and parallel loops of heating wire on an asbestos sheet. In order to get uniform radiation between the electric heater and absorber plate, 1 mm thickness mica sheet was placed over electric heater wire. A uniform heat flux of 1000 W/m^2 was maintained using variable transformer. The mass flow rate was measured using calibrated orifice meter connected with U-tube manometer. An orifice plate was designed for flow measurement in 80 mm diameter pipe. A Micro Manometer (least count of 0.01 mm) was used to measure the pressure drop across the test section. The plate temperature was measured using 12 thermocouples (28 SWG) provided over the plate and 8 thermocouples were used to measure temperature inside the duct. To measure the output of the thermocouples, a mili-voltmeter was used. A glass wool was used as insulator to reduce the heat losses from 6 mm thick wooden panel. During operation of solar air heater, mass

Table 2
The accuracy of measuring instruments used in experimental investigation.

S. No	Name of the instrument	Accuracy
1	U-tube manometer	±1 mm of Hg
2	Micro manometer	±0.03 h Pa
3	Thermocouples	±0.1 °C
4	Milli-voltmeter	±0.1 V

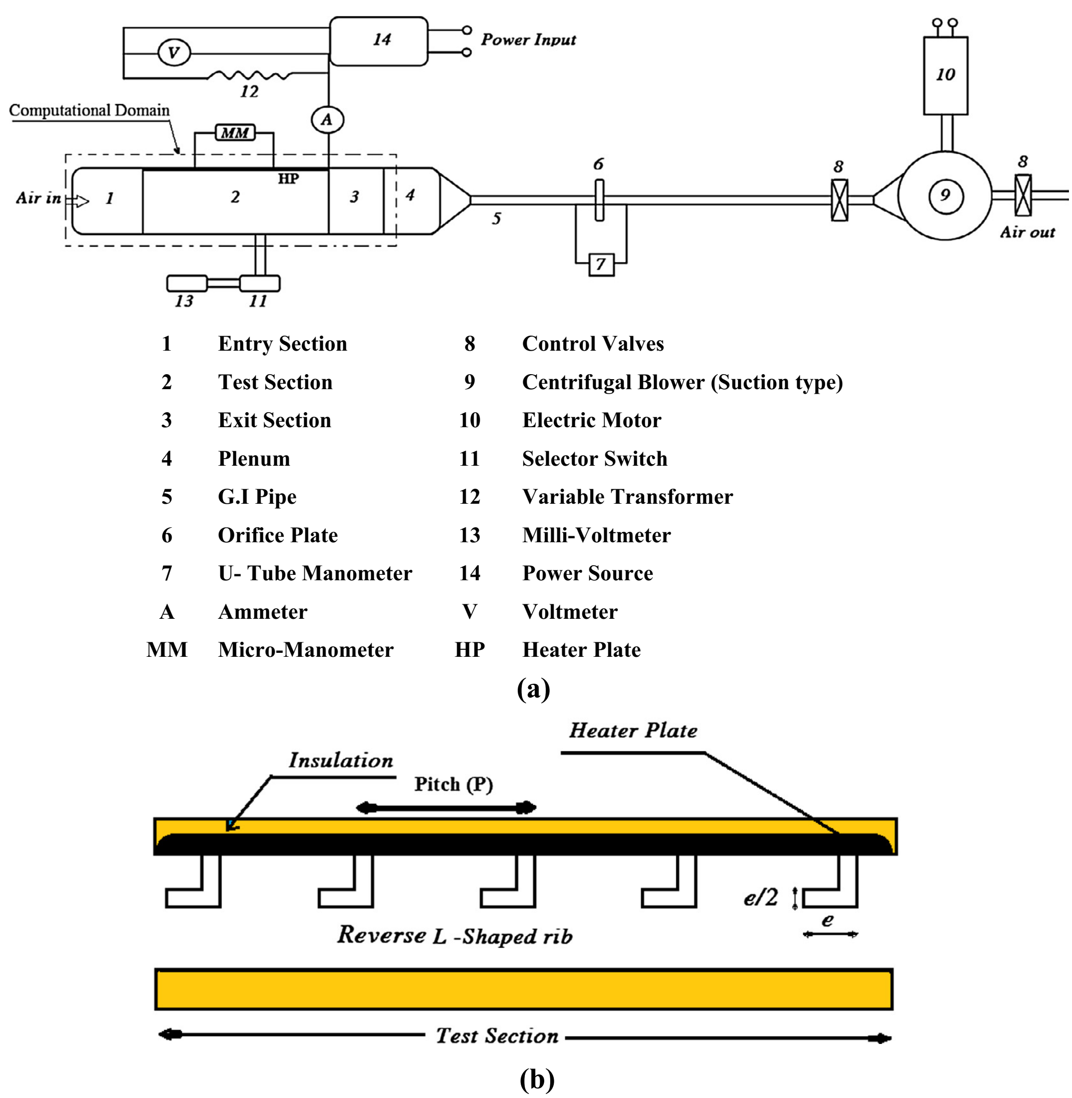

Fig. 2. (a) Schematic diagram of experimental set up for a solar air heater and (b) Test section.

flow rate in the duct was adjusted using control valve. Six values of mass flow rate were maintained to cover the entire range of Reynolds number. The accuracy of measuring instruments used in experimental analysis is mentioned in Table 2. Different configurations of reverse L-shaped rib roughness used in experimental investigation are tabulated in Table 3. The parameters measured during the experimental investigation are:

- Pressure drop across orifice plate (ΔP_0),
- Inlet air temperature (T_i),
- Outlet air temperature (T_0),
- Temperature of the plate (T_p) and
- Pressure drop across test section (ΔP_t).

2.1. Data reduction for experimental and CFD analysis

During experiments all the parameters were measured at quasi state condition. The above parameters are used to calculate Nusselt number and friction factor. Following equations are used to calculate mass flow rate 'm', heat gained by air 'Q_u' and heat transfer coefficient 'h' as follows,

$$m = C_d A_0 \sqrt{\frac{2\rho\Delta P_0}{1-\beta^4}} \tag{1}$$

The calibration of the orifice plate against Pitot tube yielded a value of 0.608 for coefficient of discharge (C_d). Where $\Delta P_0 = 9.81\ \rho_m\ \Delta h_0\ \mathrm{Sin}\,\theta$.

$$Q = m\ C_p\ (T_0 - T_i) \tag{2}$$

T_0 and T_i represent outlet and inlet air temperature. Insertion of reversed L-shaped ribs helps to increase the value of outlet fluid temperature (T_0) which in turn enhances heat transfer coefficient in solar air heater.

$$h = \frac{Q_u}{A_p(T_p - T_f)} \tag{3}$$

where A_p is heat transfer area (area of absorber plate), T_f and T_p are average values of air and absorber plate temperatures respectively. The Nusselt number (Nu) and friction factor (f) in experimental investigation and in CFD analysis were calculated by using the following relations,

$$Nu_r = \frac{hD}{k} \tag{4}$$

$$f_r = \frac{(\Delta P/l)D}{2\rho v U^2} \tag{5}$$

where D is called hydraulic diameter ($D = 4A/P$, A – cross sectional area, P – wetted perimeter of cross section). Hydraulic diameter is a term generally used in calculation of properties in non-circular tubes and channels.

The Reynolds number is expressed as,

$$Re = \frac{\rho UD}{\mu} \tag{6}$$

The optimum configuration of reverse L-shaped rib was selected using a factor called as thermo hydraulic performance parameter (THPP) defined by Webb and Eckert (1972) and is given as,

$$\mathrm{THPP} = \frac{Nu_r/Nu_s}{(f_r/f_s)^{1/3}} \tag{7}$$

In CFD analysis, Nusselt number for smooth duct (Nu_s) of a solar air heater can be obtained by the Dittus–Bolter equation (McAdams, 1942),

$$Nu_s = 0.023Re^{0.8}Pr^{0.4} \tag{8}$$

Similarly, Friction factor for smooth duct (f_s) of a solar air heater can be calculated in CFD analysis by using Blasius equation (Fox et al., 2010),

$$f_s = 0.0791Re^{-0.25} \tag{9}$$

The uncertainty analysis was performed as per the method proposed by Kline and McClintock (1953) and for roughened plate investigated in this experimental work, the uncertainties in the calculated values of various parameters are given below:

- Reynolds number = ±5.25%,
- Nusselt number = ±6.28%,
- Friction factor = ±7.15%.

3. CFD Analysis of solar air heater duct

The results of experimental investigation are compared with the CFD analysis. Two dimensional CFD analysis of solar air heater rectangular duct with reverse L-shaped ribs as artificial roughness on the underside of absorber plate is carried out using CFD code ASNSYS FLUENT 14.1. For analysis, the flow is assumed as single phase, incompressible, thermally and hydraulically fully devel-

Table 3
Different configurations of L-shaped rib roughness used in experimental investigation.

Roughness configuration	Hydraulic diameter of duct D (mm)	Rib height e (mm)	Relative roughness height, e/D	Rib pitch P (mm)	Relative roughness pitch, P/e
Type-a	33.33	1.4	0.042	10	7.14
Type-b				15	10.71
Type-c				20	14.29
Type-d				25	17.86

oped and turbulent across the duct. Thermo physical properties of air and absorber plate are assumed constant i.e. temperature independent. The radiation heat transfer from the duct is considered as negligible. The computational procedure required for the present analysis is presented in the following sub-sections.

The CFD methodology adopted in this paper can also be found in author's previous publications (Gawande et al., 2014b, 2016b,c).

3.1. Computational domain

In the numerical analysis, two dimensional computational domain of solar air has been generated using ANSYS Modeler 14.1 as shown in Fig. 3. The solution domain is a rectangular duct (Yadav and Bhagoria, 2014b), which is divided into three sections namely entry section ($L_1 = 245$ mm), test section ($L_2 = 280$ mm) and exit section ($L_3 = 115$ mm). Duct aspect ratio, (W/H) is kept as 5 by taking height of the duct as, $H = 20$ mm and width $W = 100$ mm. Hydraulic diameter of solar air heater duct is, $D = 33.33$ mm. The domain lengths are calculated according to ASHRAE Standards 93-2003 (ASHRAE Standard 93, 2003). In the test section (L_2), top wall consists of a absorber plate made of aluminum. Artificial roughness in the form of reverse L-shaped rib is considered at the underside of the top of the duct on the absorber plate. The plane containing roughness elements is kept perpendicular to the flow direction. The height of the rib is maintained at 1.4 mm, so that the fin and flow passage blockage effects may be negligible (Yadav and Bhagoria, 2013a) (as relevant in solar air heater from experimental results). A uniform heat flux of 1000 W/m^2 is applied on the top surface of test section. Pitch between two adjacent rib is maintained at 10 mm, 15 mm, 20 mm and 25 mm. Relative roughness pitch varies in the range of $7.14 \leqslant P/e \leqslant 17.86$ mm. Relative roughness height (e/D) is kept constant as 0.042. Reynolds number varies in the range of $3800 \leqslant Re \leqslant 18{,}000$, most suitable for air heater as predicted from experimental investigations (Chaube et al., 2006). Different configurations of the reverse L-shaped rib roughness used in CFD analysis are shown in Fig. 4.

3.2. Grid generation

The meshing module of ANSYS 14.1 is used for creating non-uniform mesh on the computational domain of solar air heater as shown in Fig. 5. For resolving the laminar sub layer, very fine mesh size is used near the boundary of solar air heater duct. The mesh generated for the present analysis consists of 211,582 elements and 199,816 nodes. The grid independence test is carried out by varying elements from 185,254 to 220,154 in five steps for $Re = 18{,}000$, $P/e = 7.14$ and $e/D = 0.042$. The increase in mesh elements after 211,582 has less than 1% variation in Nusselt number and fiction factor as shown in Table 4. So the mesh with 211,582 elements is taken as criterion for grid independence and is used for carrying out numerical analysis for the cases investigated in this paper.

3.3. Governing equation

Steady state two dimensional continuity, time independent incompressible Navier Stokes equation and energy equation are used to solve the fluid phenomenon in artificially roughened solar air heater rectangular duct. In the Cartesian tensor system these governing equations can be written as,

Continuity equation:

$$\frac{\partial}{\partial x_i}(\rho u_i) = 0 \tag{10}$$

Momentum equation

$$\frac{\partial}{\partial x_i}(\rho u_j u_j) = -\frac{\partial p}{\partial x_i} + \frac{\partial}{\partial x_j}\left[\mu\left(\frac{\partial u_i}{\partial x_j} + \frac{\partial u_j}{\partial x_i}\right)\right] + \frac{\partial}{\partial x_j}\left(-\rho\overline{u_i' u_j'}\right) \tag{11}$$

Energy equation

$$\frac{\partial}{\partial x_i}(\rho u_j T) = \frac{\partial}{\partial x_j}\left((\Gamma + \Gamma_t)\frac{\partial T}{\partial x_j}\right) \tag{12}$$

where Γ and Γ_t are the molecular thermal diffusivity and turbulent thermal diffusivity respectively and are given by,

$$\Gamma = \mu/Pr \quad \Gamma_t = \mu_t/Pr_t \tag{13}$$

Eqs. (1) and (2) are also called as Reynolds-averaged Navier–Stokes equations.

Transport equations used for Renormalization-group (RNG) k–ε model, to determine turbulence kinetic energy, k and rate of dissipation, ε for computational domain analysis are:

$$\frac{\partial}{\partial x_i}(\rho k u_i) = \frac{\partial}{\partial x_j}\left(\alpha_k \mu_{eff}\frac{\partial k}{\partial x_j}\right) + G_k - \rho\varepsilon \tag{14}$$

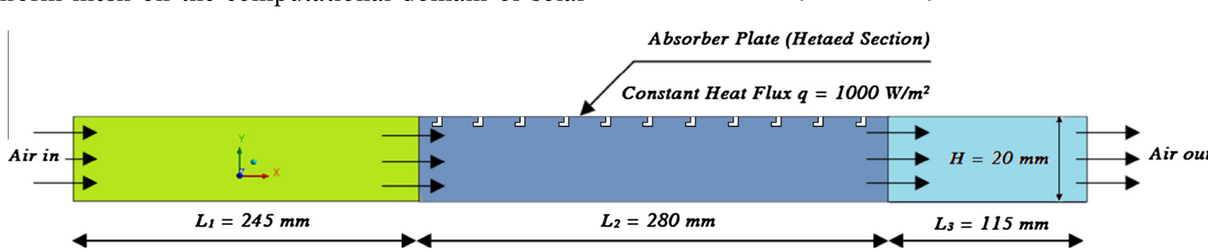

Fig. 3. Schematic of two-dimensional domain of solar air heater.

and

$$\frac{\partial}{\partial x_i}(\rho\varepsilon u_j) = \frac{\partial}{\partial x_j}\left(\alpha_k \mu_{eff}\frac{\partial\varepsilon}{\partial x_j}\right) + C_{1\varepsilon}\frac{\varepsilon}{k}(G_k) - C_{2\varepsilon}\rho\frac{\varepsilon^2}{k} - R_\varepsilon \quad (15)$$

where G_k represents the generation of turbulence kinetic energy due to mean velocity gradients and is expressed as,

$$G_k = -\rho\overline{u_i' u_j'}\frac{\partial u_j}{\partial x_i} \quad (16)$$

μ_{eff} represents the effective turbulent viscosity and is given as,

$$\mu_{eff} = \mu + \mu_t \quad (17)$$

The turbulent viscosity, μ_t is computed by combining k and ε as follows:

$$\mu_t = \rho C_\mu \frac{k^2}{\varepsilon} \quad (18)$$

where $C_\mu = 0.0845$ is constant.

The quantities α_k and α_ε are the inverse effective turbulent Prandtl numbers for k and ε respectively. The model constants have the following values, $C_{1\varepsilon} = 1.42$, $C_{21\varepsilon} = 1.68$, $\alpha_k = 1.39$ and $\alpha_\varepsilon = 1.39$.

3.4. Boundary condition

The solution domain of solar air heater is a rectangular duct with inlet, test and exit sections. The working fluid used in solar air heater duct is air and the absorber plate is 0.5 mm thick and made up of aluminum. The thermo physical properties of air and absorber plate material as shown in Table 5, have been assumed to remain constant at average bulk temperature. A constant heat flux of 1000 W/m^2 is maintained on the top wall of test section. At inlet, uniform velocity boundary condition is applied and fixed pressure (1.013×10^5 Pa) outlet boundary condition is applied at the exit. Other solid surfaces are maintained at no-slip boundary condition and turbulence kinetic energy is set to zero on all solid walls. At inlet, tur-

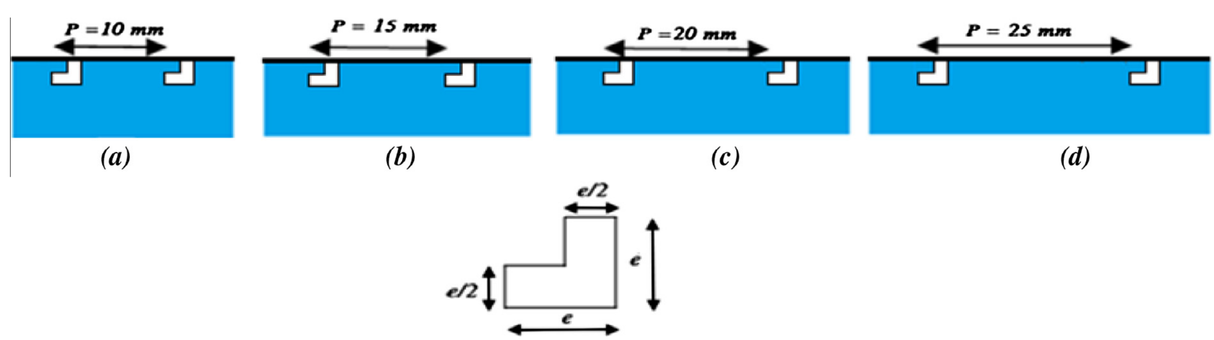

Fig. 4. Variation of pitch and details for reverse L-shaped rib roughness on absorber plate.

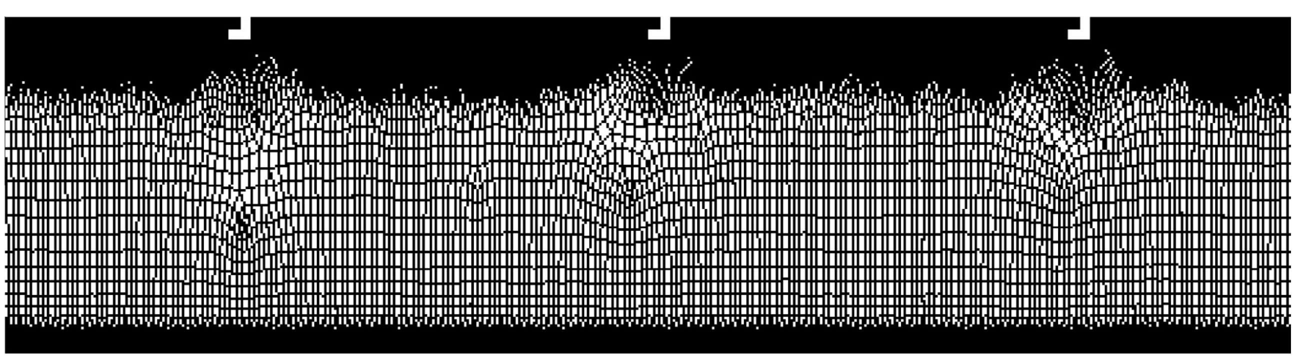

Fig. 5. Non-uniform grid for computational domain of solar air heater with reverse L-shaped ribs roughness.

Table 4
Grid independence test for CFD analysis.

S. No	Number of elements	Nusselt number (Nu)	% Difference	Friction factor (f)	% Difference
1	185,254	149.33	–	0.0237	–
2	195,269	152.28	1.95	0.0246	3.72
3	199,358	153.04	0.49	0.0249	1.21
4	211,528	152.75	0.18	0.0250	0.40
5	220,154	152.95	0.13	0.0251	0.39

bulence intensity suggested in ANSYS 14.1 (Fluent, 2012) is applied and is calculated as,

$$I = 0.16\ (Re)^{-1/8}$$

3.5. Solution method

The CFD analysis of solar air heater duct with reverse L-shaped artificial roughness is carried out using CFD code ANSYS FLUENT 14.1. The flow chart for the numerical simulation with CFD in solar air heater is as follows:

- Define modeling goals,
- Extract computational domain from actual set up,
- Create solid model of the domain,
- Mesh/grid generation on domain,
- Set up solver,
- Compute the solution,
- Examine the results,
- Modify the domain and repeat analysis (revisions to the model).

In first step of defining modeling goals, in present analysis, we are concerned with the properties like mass flow rate, pressure, temperature, etc. Two-dimensional domain is selected over three dimensional, since it saves computational time and results are in good agreement with results of three dimensional domain analysis. Then computational domain is selected from the physical system as shown in Fig. 3. CAD model of computational domain is prepared in ANSYS modeler 14.5 and non uniform grid is generated to capture gradients. Material properties, operating conditions, boundary conditions, solver controls and convergence monitors are set up in solver (FLUENT). In solver, governing flow equations are converted into system of algebraic equations. This stage is known as discretization stage. The governing equations of continuity, momentum and energy are discretized using finite volume method (FVM). In FVM, the solution domain is subdivided into finite number of small control volumes by grid. The boundaries of the control volume are defined by the grid while the computational node lies at the center of the control volume. The flow equations are solved using RNG k–ε turbulence model as it shows very good agreement with the empirical relations as shown in Fig. 6. A second order scheme is selected for energy and momentum equations. To couple pressure and velocity, SIMPLE algorithm is selected, as described by Patankar (1980). The convergence criteria of 10^{-3} for the residuals of continuity equations, 10^{-6} for the residuals of velocity components and 10^{-6} for the residuals of energy are selected in FLUENT 14.1. The discretized conservation equations are solved iteratively until convergence. The results are examined to review solution and extract useful data. After examining the results, necessary revisions or modifications are made in the domain to obtain results with different operating condition.

Table 5
Thermo physical properties of air and absorber plate used for CFD analysis.

Properties	Air	Absorber plate (aluminum)
Specific heat 'C_p' (J kg^{-1} K^{-1})	1006.43	871
Thermal Conductivity 'k' (Wm^{-1} K^{-1})	0.0242	202.4
Density 'ρ' (kg m^{-3})	1.225	2719
Viscosity 'μ' (N m^{-2})	1.7894e^{-05}	–

4. Result and discussion

The experimental investigation and CFD analysis of two dimensional domain of a solar air heater of same size was carried out to study the effect of reverse L-shaped rib fitted on the underside of an absorber plate of solar air heater. The effect of relative roughness pitch and Reynolds number was studied on the heat transfer and friction characteristics of solar air heater. The results obtained from experimental investigation and comparison between CFD and experimental results are explained in the following subsection.

4.1. Validity test for smooth channel

The experimental results are validated by comparing the results obtained for smooth duct with the Dittus Bolter (McAdams, 1942) and Blasius (Fox et al., 2010) equation as shown in Fig. 7(a) and (b). A reasonable good agreement between the experimental and predicted values ensures the accuracy of the data being collected with the help of experimental set up.

4.2. Heat transfer characteristics

The insertion of reverse L-shaped ribs as artificial roughness on the underside of an absorber plate of a solar air heater duct causes increase in heat transfer enhancement. Fig. 8 shows the effect of Reynolds number on average Nusselt number for different values of relative roughness pitch at constant relative roughness height. The presence of reverse L-shaped ribs as artificial roughness produces enhancement in heat transfer than that of smooth duct. It can be seen that the average Nusselt number increases with the increase in Reynolds number as shown in Fig. 9. The heat transfer rate increases with the increase in Reynolds number due to increase in velocity with the increase in Reynolds number. The contour plots of velocity from CFD analysis for various relative roughness pitches at $Re = 12{,}000$, are shown in Fig. 10. The increase in Reynolds number decreases laminar sub layer thickness. The increase turbulence generated due to increase in velocity creates vortices around top surface of reverse L-shaped rib, which transfers heat from the hot

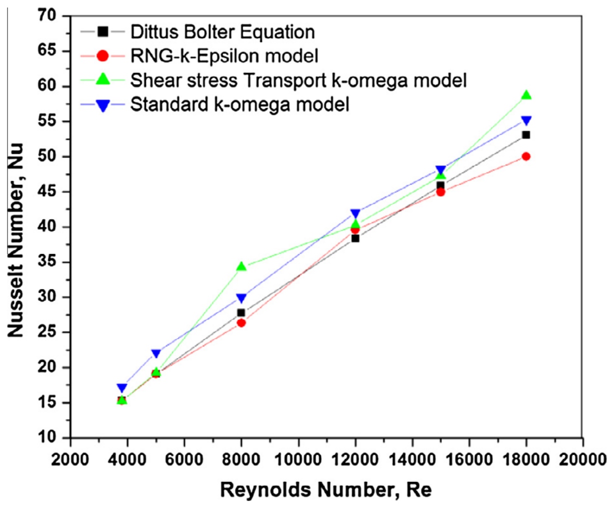

Fig. 6. Comparison between Nusselt number predictions using Dittus Bolter empirical correlation and different turbulence model in FLUENT for smooth duct.

absorber plate to the core cold fluid. The reverse L-shaped arrangement disturbs the development of boundary layer. This causes increase in turbulent kinetic energy and turbulent intensity. The contours plots of turbulent kinetic energy and turbulent intensity obtained from CFD analysis are shown in Figs. 11 and 12. Turbulent kinetic energy is defined as the mean kinetic energy per unit mass associated with eddies in turbulent flow. Turbulence kinetic energy directly represents the strength of the turbulence in the flow field. Turbulence intensity is also a measurement of turbulence expressed as a percent. The contour plots of turbulent kinetic energy and turbulent intensity helps to understand the thermal phenomenon of artificially roughened solar air heater with reverse L-shaped rib as artificial roughness. The contour plot of turbulent kinetic energy and turbulent intensity shows that the maximum value of turbulent kinetic energy and turbulent intensity is predicted near

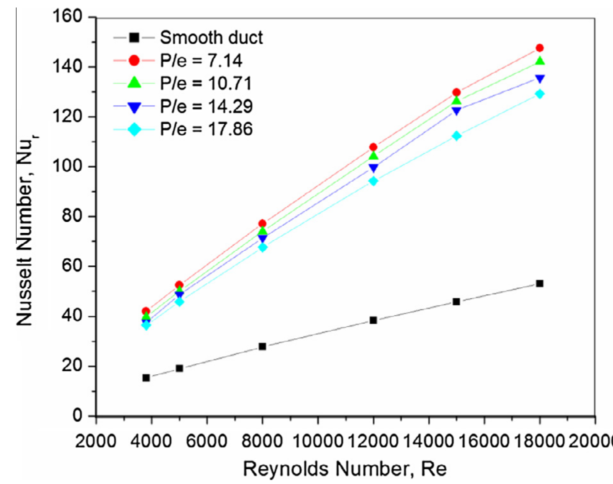

Fig. 8. Variation of average Nusselt number for different values of relative roughness pitch and for fixed value of relative roughness height versus Reynolds number.

the absorber plate and between the region of first and second rib and then it decreases with the increase in distance from the absorber plate. The tip of the L-shaped rib develops higher turbulence at the entry. Stronger the turbulence, stronger is the shear. Also at the inlet the flow is developing and hence the shear in the boundary layer is predominant and hence turbulent intensity value is higher in the vicinity of first rib. As the flow becomes fully developed, the shear in the boundary layer decreases moving away from the absorber plate and hence turbulence intensity is also decreases. Also the detachment of the flow reduces shear in the boundary layer. The heat transfer increases with the increase in turbulent intensity as intensity of shear layer is greater in the neighborhood of the ribs as compared to that in smooth solar air heater. The repeating Nusselt number distribution along the stream wise direction is generated due to flow reattachment and presence of high turbulence kinetic energy level between a pair of ribs.

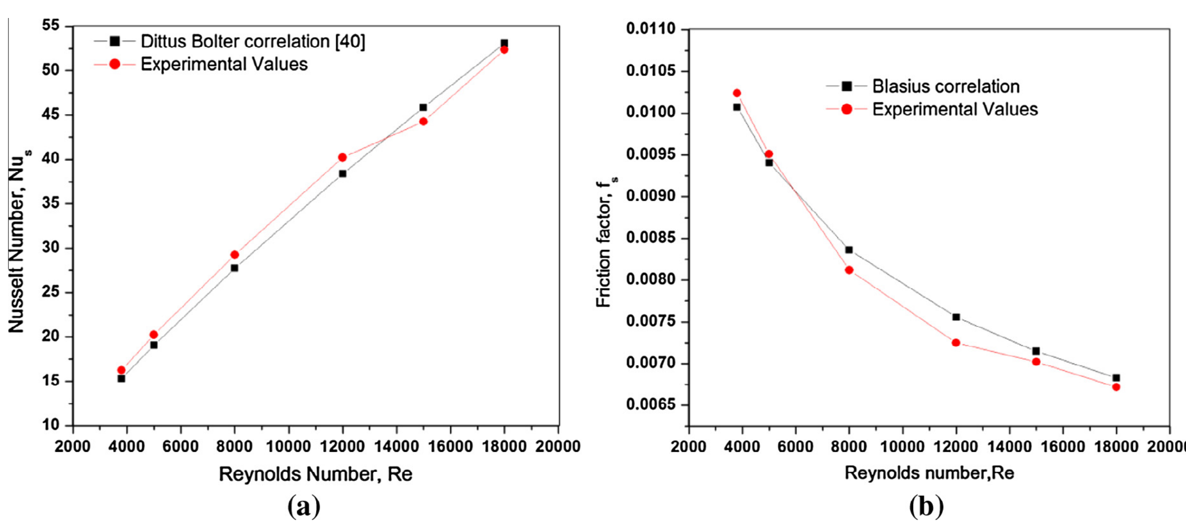

Fig. 7. Comparison of experimental and predicted values of (a) Nusselt number and (b) friction factor for smooth duct.

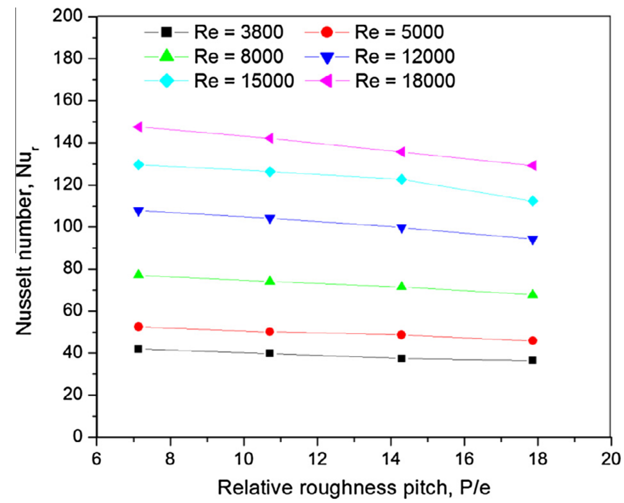

Fig. 9. Effect of Reynolds number on average Nusselt number for different values of relative roughness pitch for fixed value of relative roughness height.

The heat enhancement occurs due to strong downwards flow and the high momentum cold fluid to the ribbed walls. The comparison between contour plots of turbulence kinetic energy and turbulent intensity for square rib and reverse L-shaped roughness is shown in Fig. 13 and Fig. 14 respectively. From figure it has been observed that, eddies formation are more predominant on tip of the rib and in between the ribs in case of reversed L-shaped rib. As compared to square rib, reverse L-shaped rib generates more fluctuations in the flow and hence intensity of turbulence and turbulence kinetic energy increases with insertion of these ribs. Hence heat transfer enhances in a solar air heater with reversed L-shaped roughness.

Fig. 8 also shows that average Nusselt number tends to increase as the relative roughness pitch decreases for fixed value of relative roughness height. The decrease in relative roughness pitch increases the reattachment points due to presence of maximum number of ribs spacing on the absor-

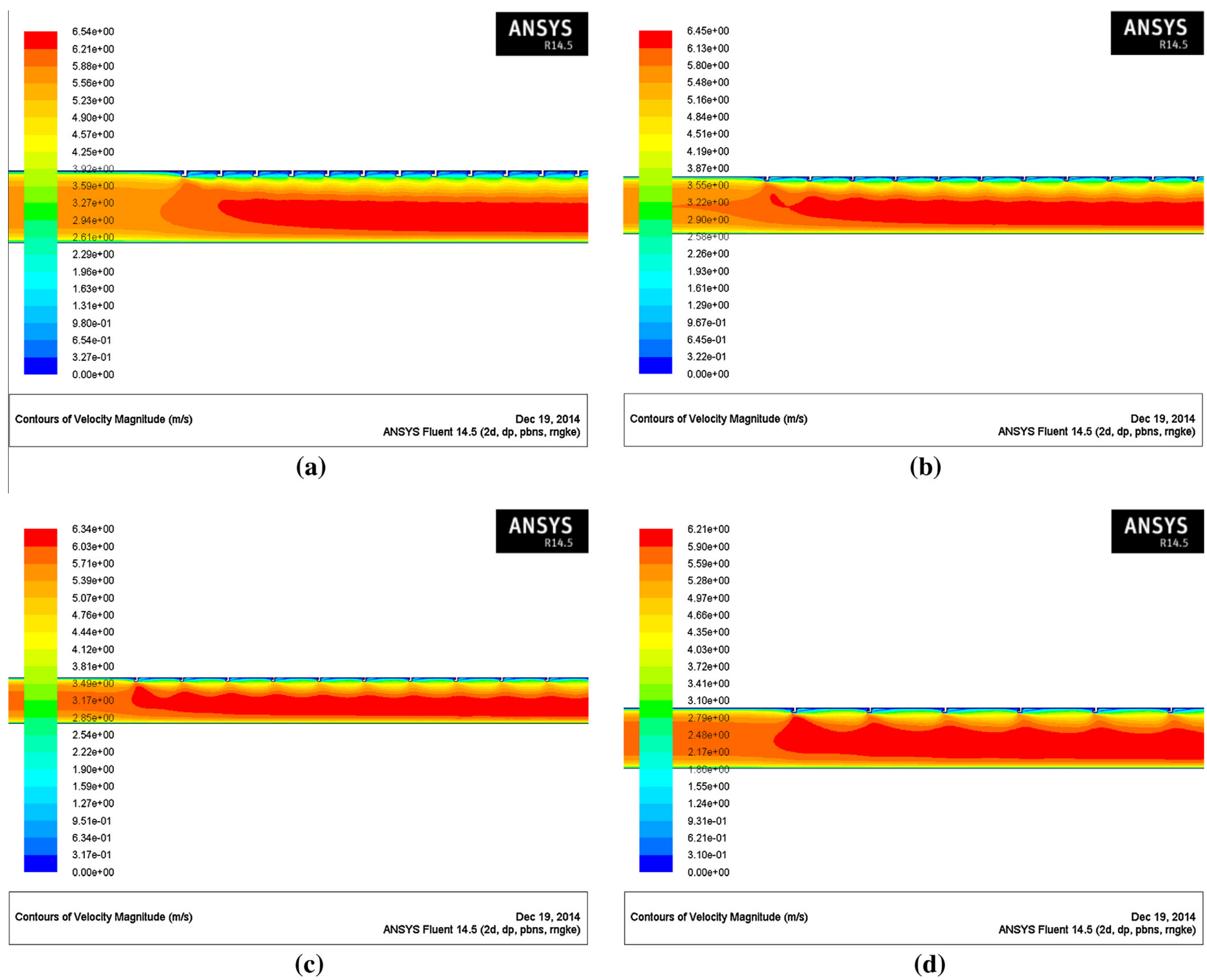

Fig. 10. The contour plots of velocity from CFD analysis for $Re = 12{,}000$ and at roughness pitch (a) $P/e = 7.14$, (b) $P/e = 10.71$, (c) $P/e = 14.29$ and (d) $P/e = 17.86$.

ber plate. The decrease in relative roughness pitch increases average turbulent intensity and flow acceleration. This leads to increase in average Nusselt number. As the value of relative roughness pitch increases, the numbers of ribs on the absorber plate decreases which cause decrease in reattachment points on the absorber plate. The increase

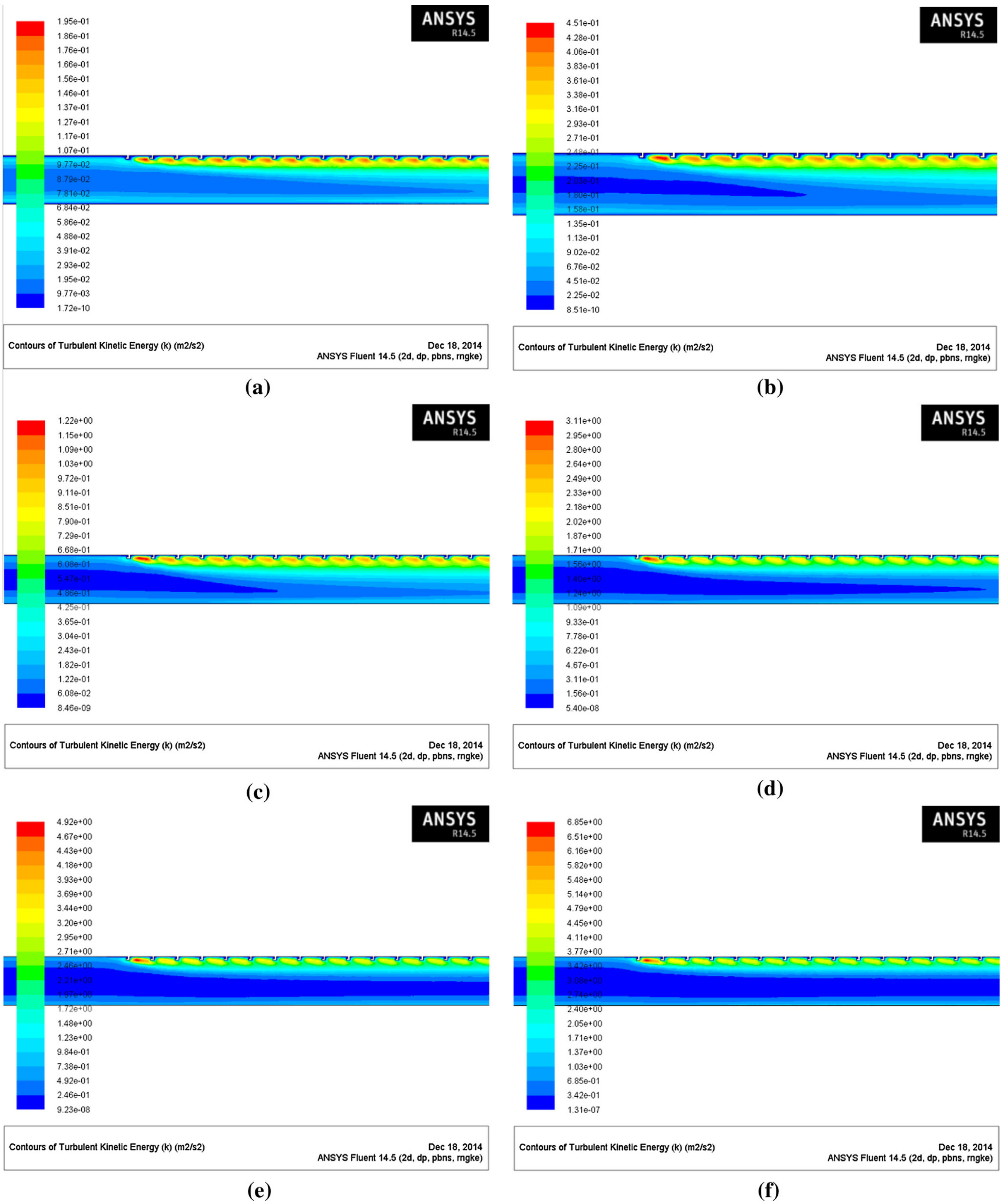

Fig. 11. The contour plot of turbulent kinetic energy using CFD for $e/D = 0.042$ and $P/e = 7.14$ at a Reynolds number of (a) 3800, (b) 5000, (c) 8000, (d) 12,000, (e) 15,000 and (f) 18,000.

of relative roughness pitch decreases heat transfer in solar air heater duct. The experimental data plotted in Fig. 8, shows that, maximum enhancement in Nusselt number is obtained at relative roughness pitch of 7.14 at $Re = 15{,}000$. The maximum enhancement in the Nusselt number is found to be 2.827 times over the smooth duct

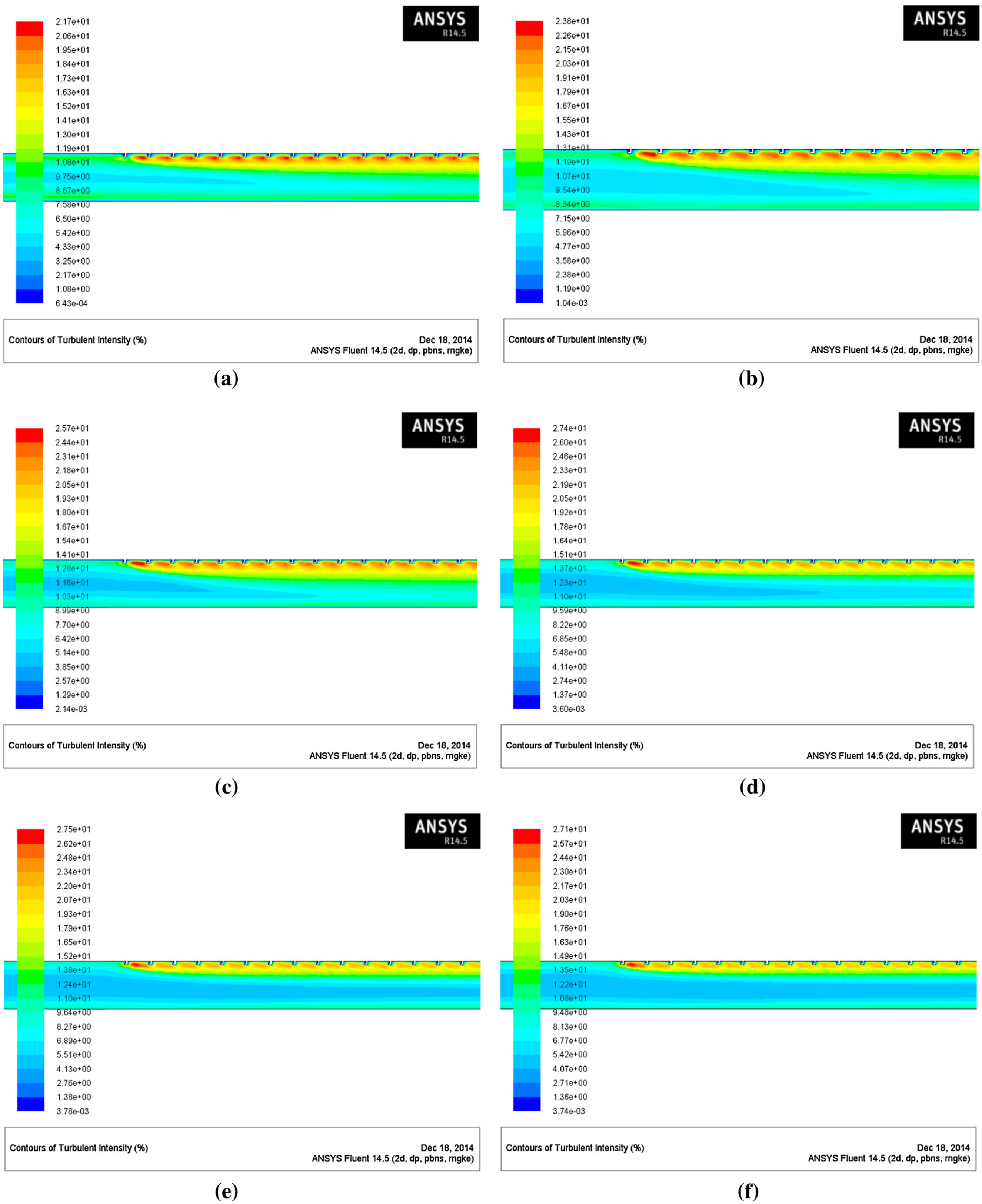

Fig. 12. The contour plot of turbulent intensity using CFD for $e/D = 0.042$ and $P/e = 7.14$ at a Reynolds number of (a) 3800, (b) 5000, (c) 8000, (d) 12,000, (e) 15,000 and (f) 18,000.

corresponding to relative roughness pitch of 7.14 at constant relative roughness height of 0.042. The enhancement in average Nusselt number over the smooth duct for different value of relative roughness pitch at constant relative roughness height are tabulated in Table 6.

4.3. Flow friction characteristics

Fig. 15 shows the effect of Reynolds number on average friction factor for different values of relative roughness pitch at constant relative roughness height. The insertion of reverse L-shaped rib as artificial roughness on the absorber plate of solar air heater creates obstruction in the flow. This results in high pressure drop due to boundary layer separation and reattachment. The increased in pressure drop results in increased friction factor in roughened solar air heater duct as compared to smooth duct. Increase in Reynolds number causes suppression of laminar sub layer and hence the friction factor values decreases as Reynolds number increases as shown in Fig. 16. As discussed in

Table 6
Nusselt number enhancement ratio for varying Reynolds number and pitch at constant P/e and e/D.

$D = 33.33$ mm				Nusselt number enhancement ratio (Nu_r/Nu_s) Reynolds number					
e (mm)	e/D	P (mm)	P/e	3800	5000	8000	12,000	15,000	18,000
1.4	0.042	10	7.14	2.742	2.753	2.781	2.808	2.827	2.780
		15	10.71	2.600	2.630	2.670	2.715	2.754	2.678
		20	14.29	2.450	2.555	2.577	2.599	2.674	2.556
		25	17.86	2.383	2.408	2.440	2.457	2.449	2.434

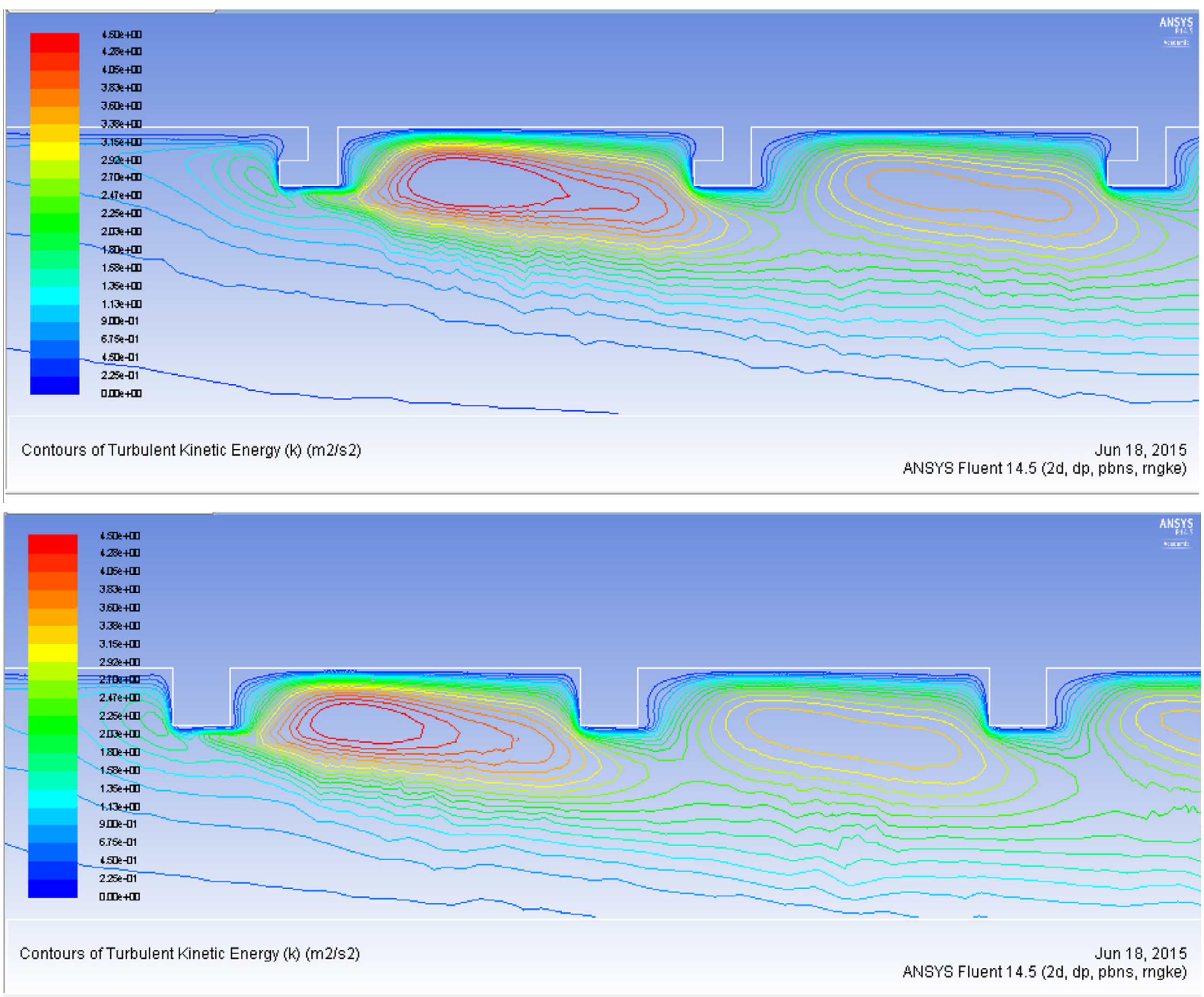

Fig. 13. Contour plots of turbulence kinetic energy for reversed L-shaped and square rib roughness.

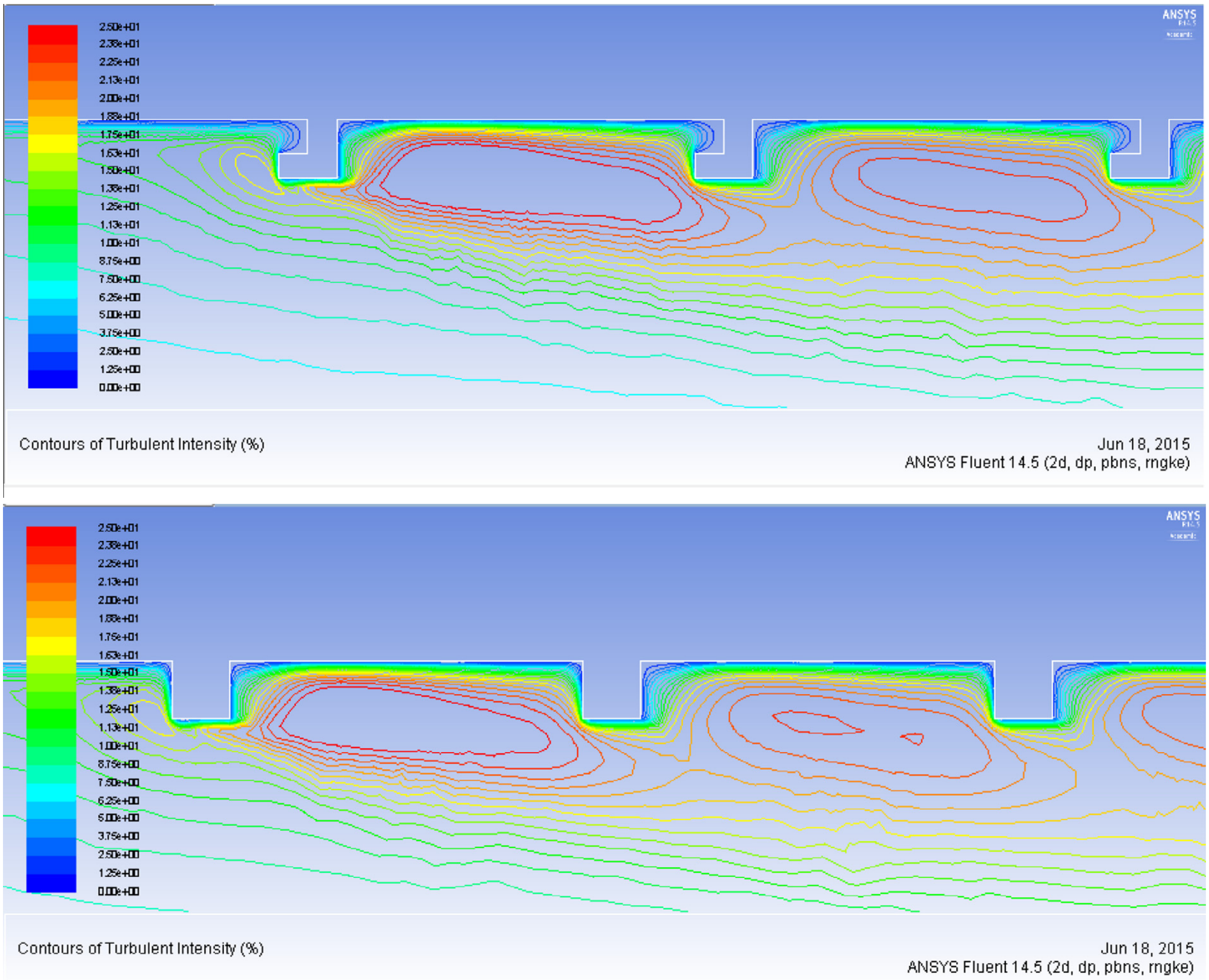

Fig. 14. Contour plots of turbulent intensity for reversed L-shaped and square rib roughness.

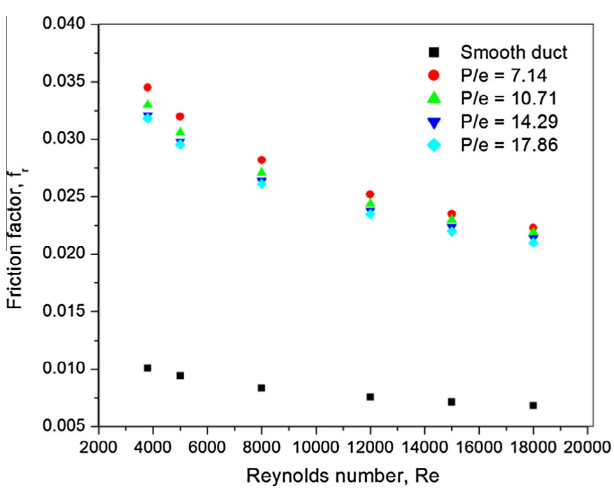

Fig. 15. Variation of average friction factor for different values of relative roughness pitch and for fixed value of relative roughness height versus Reynolds number.

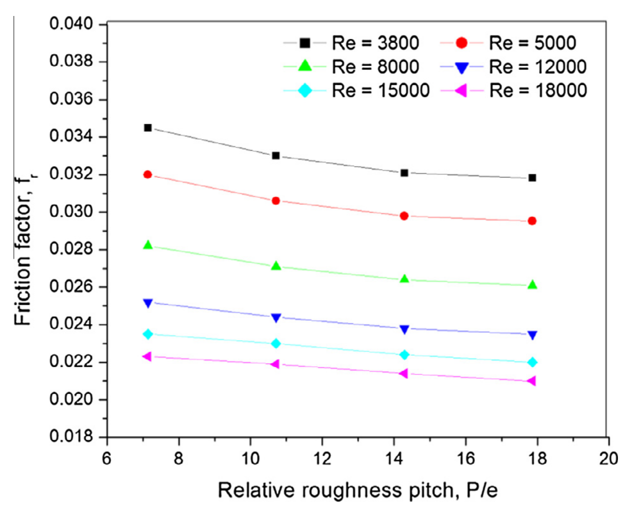

Fig. 16. Effect of Reynolds number on average friction factor for different values of relative roughness pitch for fixed value of relative roughness height.

above section, increase in Reynolds number, increases turbulent intensity and hence heat transfer increases with less value of friction factor.

The effect of relative roughness pitch for fixed value of relative roughness height, on the average friction factor, for different Reynolds number is shown in Fig. 15. It is

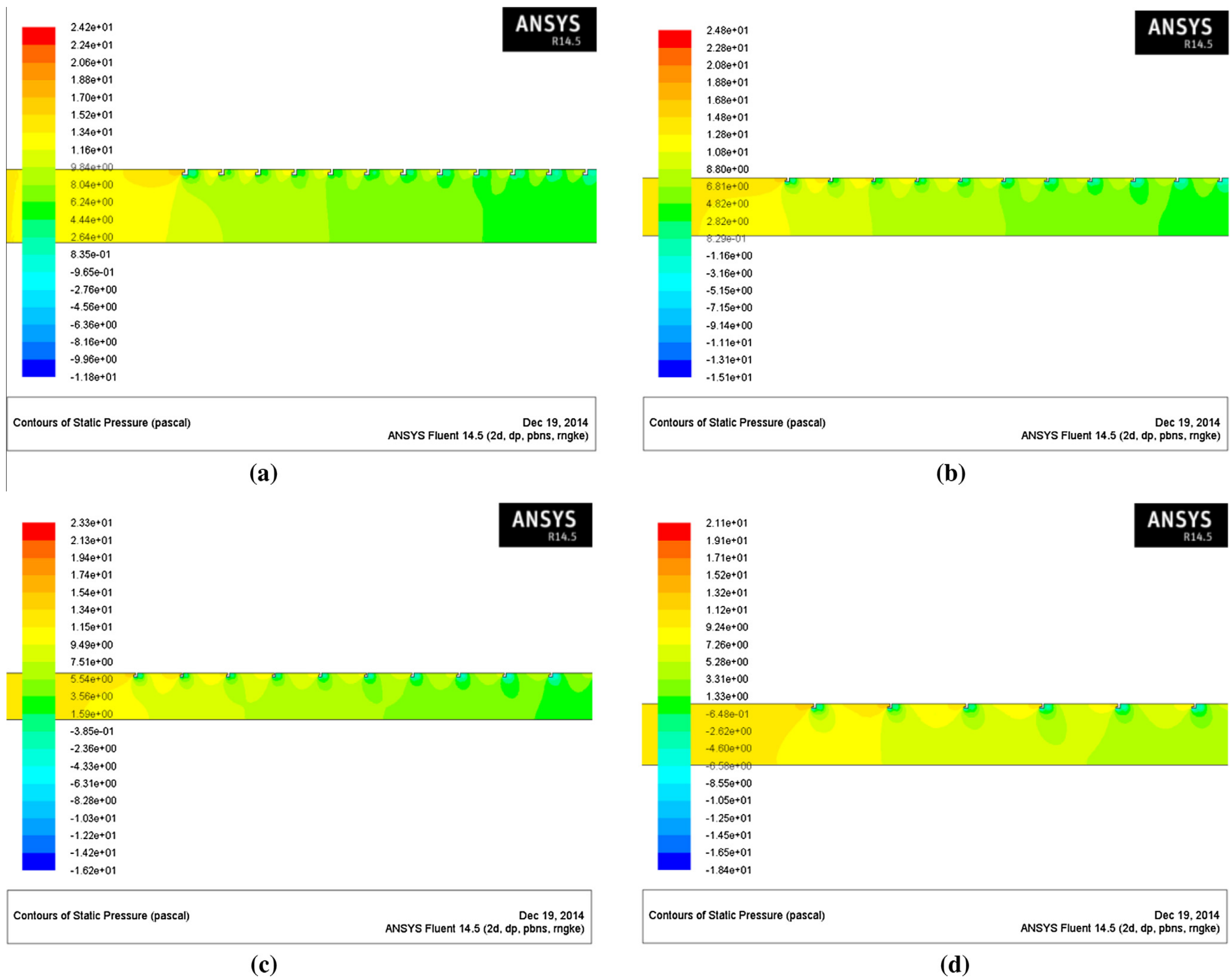

Fig. 17. The contour plots of pressure at $Re = 12{,}000$ at relative roughness pitch of $P/e = 7.14$, (b) $P/e = 10.71$, (c) $P/e = 14.29$ and (d) $P/e = 17.86$.

Table 7
Friction factor enhancement ratio for varying Reynolds number and pitch at constant P/e and e/D.

$D = 33.33$ mm				Friction factor enhancement ratio (f_r/f_s) Reynolds number					
e (mm)	e/D	P (mm)	P/e	3800	5000	8000	12,000	15,000	18,000
1.4	0.042	10	7.14	3.424	3.402	3.372	3.334	3.288	3.265
		15	10.71	3.272	3.253	3.240	3.229	3.218	3.207
		20	14.29	3.186	3.168	3.156	3.149	3.137	3.134
		25	17.86	3.159	3.139	3.121	3.109	3.078	3.075

observed that the average friction factor tends to increase as the relative roughness pitch decreases for given fixed value of relative roughness height. The decrease in relative roughness pitch increases the number of interruptions in the flow which leads to develop high pressure drop in the system due to additional momentum loss. The contour plots of pressure using CFD analysis for $Re = 12{,}000$ and $e/D = 0.042$ at relative pitch of 10 mm, 15 mm, 20 mm and 25 mm are shown in Fig. 17. The number of interruptions decreases with increases in relative roughness pitch and hence average friction factor decreases with increase in relative roughness height. The reverse L-shaped rib roughness with relative roughness pitch of 7.14 provides maximum value of average friction factor at $Re = 3800$ for fixed value of relative roughness height. Thus it can be concluded that the average friction factor is dependent on the relative roughness pitch of reverse L-shaped ribs roughness along with the variation of Reynolds number. The friction factor enhancement ratio is a factor which relates the enhancement in average friction factor of roughened solar air heater duct with the smooth duct. The maximum enhancement in friction factor is found to be 3.424 times over the smooth duct corresponding to relative roughness pitch of 7.14. The enhancement in average friction factor over the smooth duct for different values of relative roughness pitch and at constant value of relative roughness height is presented in Table 7.

4.4. Thermo-hydraulic performance evaluation

The presence of reverse L-shaped rib as artificial roughness on the absorber plate of solar air heater interrupts the laminar sub layer due to flow separation and reattachment between the consecutive rectangular and triangular ribs roughness elements which reduces thermal resistance. This reduction of thermal resistance in the domain increases heat transfer inside solar air heater duct. However the use of artificial roughness also increases pressure drop which in turn leads to greater pumping power requirement. So to get maximum heat transfer with minimum penalty of pumping power, the turbulence must be generated in the region very close to the absorber plate where laminar sub layer exist. The experimental and CFD investigation carried out in solar air heater using reverse L-shaped rib as artificial roughness shows the maximum heat transfer enhancement at relative roughness pitch of 7.14 and at Reynolds number of 15,000. Similarly at same relative roughness pitch of 7.14 and at Reynolds number of 3800, the maximum value of average friction factor is observed in both CFD and experimental analysis. Therefore it is necessary to determine the optimum value of rib configuration which provides maximum heat transfer at minimum friction losses. A parameter defined by Webb and Eckert (1972) known as thermo-hydraulic performance parameter (THPP) provides thermal and hydraulic performance of the system under consideration. The value of this parameter higher than one indicates usefulness of applying artificial roughness and it also helps to compare the performance of number of arrangements of reverse L-shaped rib, to select the best among them. The variation of thermo-hydraulic performance parameter (THPP) with Reynolds number for different values of relative roughness pitch (P/e) at constant relative roughness height (e/D) is shown in Fig. 18.

From experimental plotted data of Fig. 18, it has been observed that the value of thermo hydraulic performance parameter varies between 1.62 and 1.90 within the range of parameters investigated. It has been observed that solar air heater roughened with reverse L-shaped rib as artificial roughness elements with $P/e = 7.14$, $e/D = 0.042$ and $Re = 15,000$ provide better thermo hydraulic performance parameter for the range of parameters investigated for solar air heater using both CFD and experimental analysis. To validate the THPP result for particular relative roughness pitch of 7.14, CFD analysis of roughened duct was carried out with relative roughness pitch (P/e) below 7.14 i.e. at $P/e = 3.57$ at $Re = 15,000$. The comparison of contour plots for turbulent kinetic energy and turbulent intensity are plotted and is shown in Figs. 19 and 20 respectively. The comparison shows that the values are slightly predominant in the analysis carried out with $P/e = 7.14$ than $P/e = 3.57$.

4.5. Validation of model

The experimentally investigated, average Nusselt number and friction factor of a solar air heater with reverse L-shaped rib roughness mounted on absorber plate is validated with the CFD results under similar experimental operating conditions and is shown in Fig. 21. It has been found that the numerical results are in good agreement with the experimental results and are slightly under-predicted. The discrepancies for the Nusselt and friction factor values between the numerical results using RNG $k–\varepsilon$ turbulence model and the experimental results are less than ±15%.

Apart from this, to confirm the validity of the present computational model, grid independence test is carried out for five set of elements and enhancement in Nusselt number and friction factor values are observed. The grid which shows a difference of less than 1% in two consecutive sets of results is selected for the present analysis. The turbulence model in the CFD code ANSYS FLUENT is selected so that it should provide results very close to experimental results. The numerical analysis carried out by Yadav and Bhagoria (2014b), shows that the results given by RNG $k–\varepsilon$ turbulence model are in good agreement with the experimental results, for the similar range of parameters considered for the experimental investigation. As per the literature review (Alam et al., 2014), the value of relative roughness pitch in the range of 6–10 provides better thermo hydraulic performance for roughened duct. The CFD and experimental results shows that maximum heat transfer enhancement is observed for $P/e = 7.14$ which falls in between the accepted range of 6–10. Further, according

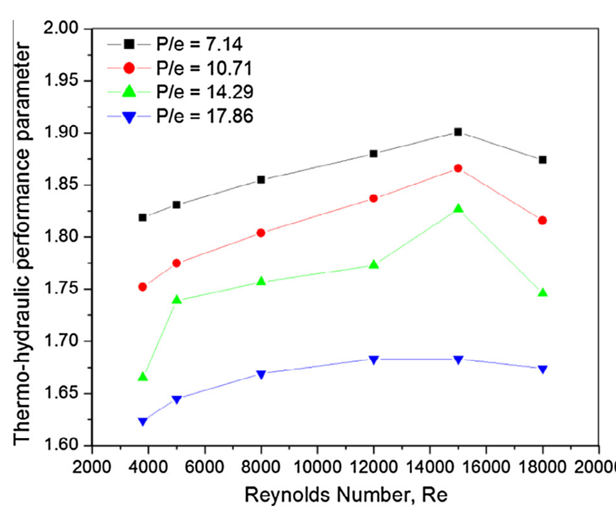

Fig. 18. Variation of thermo-hydraulic performance parameter (T.H.P.P) with Reynolds number for different values of relative roughness pitch (P/e) at constant relative roughness height (e/D).

to literature survey (Alam et al., 2014) in this area, the value of relative roughness height must lie in the range of 0.030–0.047 for better thermo hydraulic performance. The value for the present experimental and CFD analysis is also considered as 0.042 which in the accepted range for relative roughness height.

5. Development of correlations for Nusselt number and friction factor

The correlations are useful for the prediction of thermo hydraulic performance or to determine the optimum geometric parameters for a particular application. In our analysis, Nusselt number and fiction factor are strong functions of Reynolds number (Re) and relative roughness pitch (P/e) evaluated at constant relative roughness height (e/D). The functional relationship for Nusselt number and friction factor is therefore written as,

$$Nu = f_n(Re, P/e) \quad (19)$$

$$f = f_n(Re, P/e) \quad (20)$$

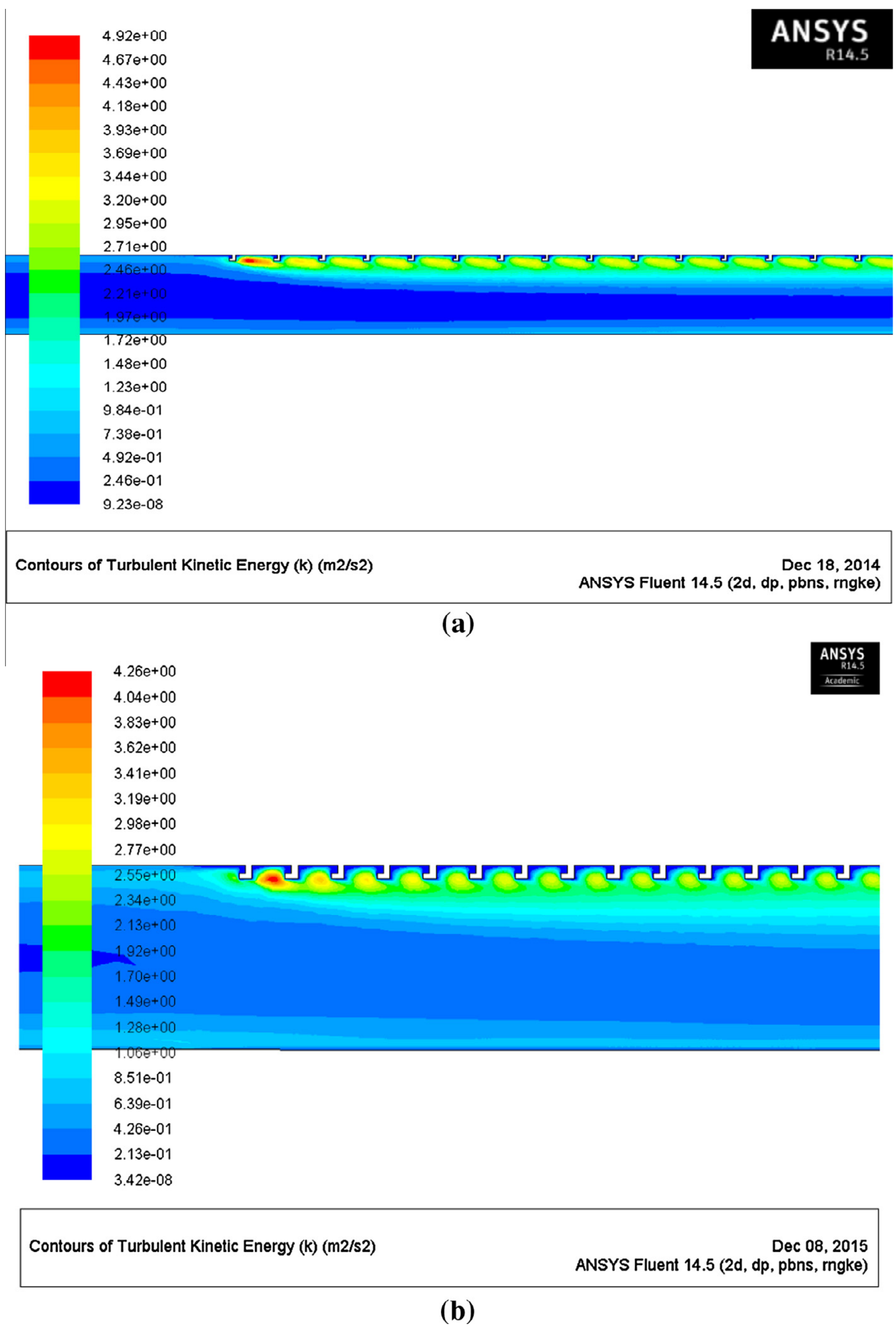

Fig. 19. Variation of turbulent kinetic energy at (a) $P/e = 7.14$ and (b) $P/e = 3.57$ at $Re = 15{,}000$.

A regression analysis to fit a straight line through the data points obtained through experimental investigations of roughened solar air heater yields the following power law relation between Nusselt number (Nu) and Reynolds number (Re) and is shown in Fig. 22(a).

$$Nu = A_0 Re^{0.8332} \tag{21}$$

The functional relationship between the Nusselt number and relative roughness pitch (P/e) was found to follow the equation as given below:

$$A_0 = B_0 (P/e)^{0.3479} \tag{22}$$

$$\text{Or} \quad \frac{Nu}{Re^{0.8332}} = B_0 (P/e)^{0.3479} \tag{23}$$

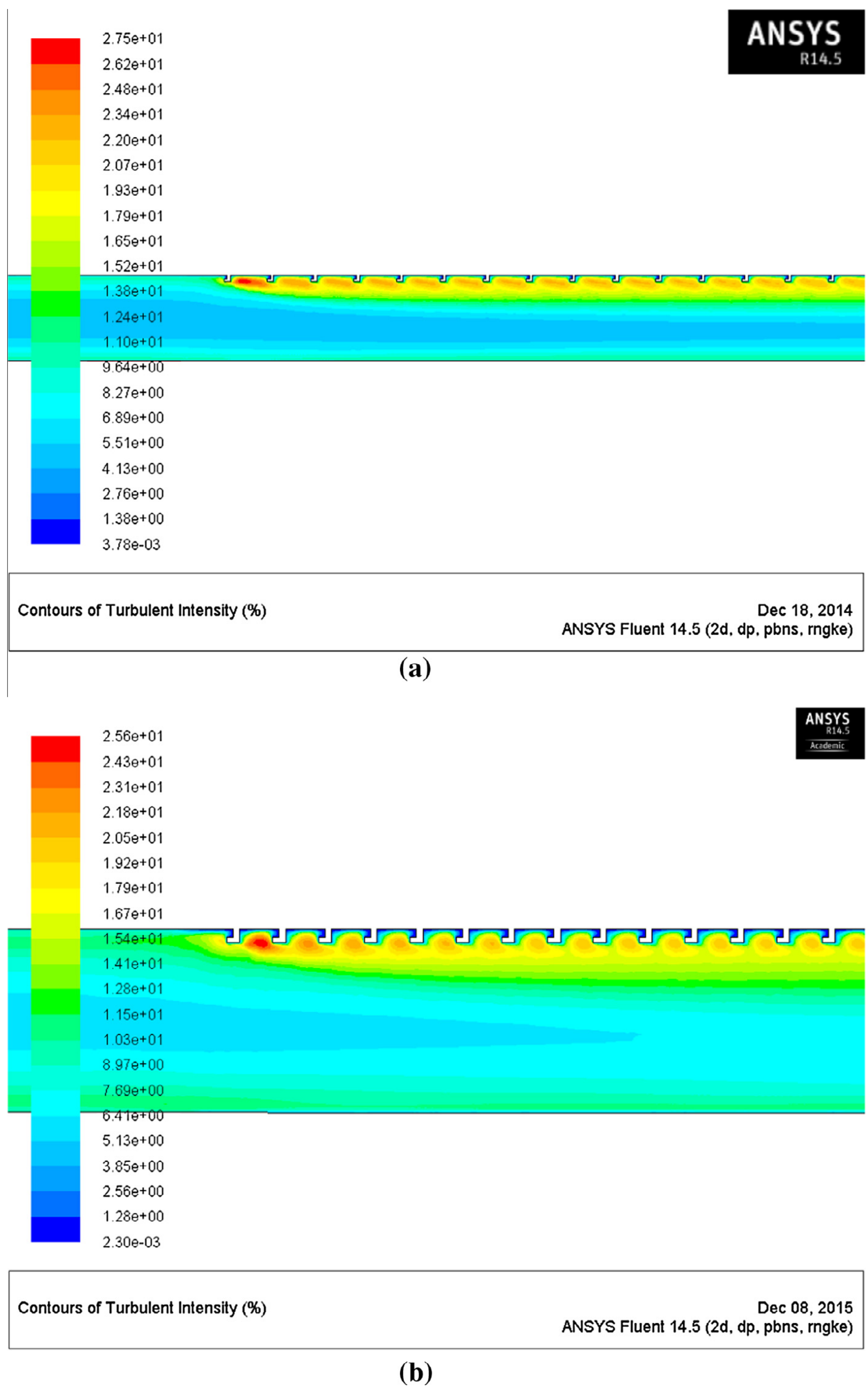

Fig. 20. Variation of turbulent intensity at (a) $P/e = 7.14$ and (b) $P/e = 3.57$ at $Re = 15{,}000$.

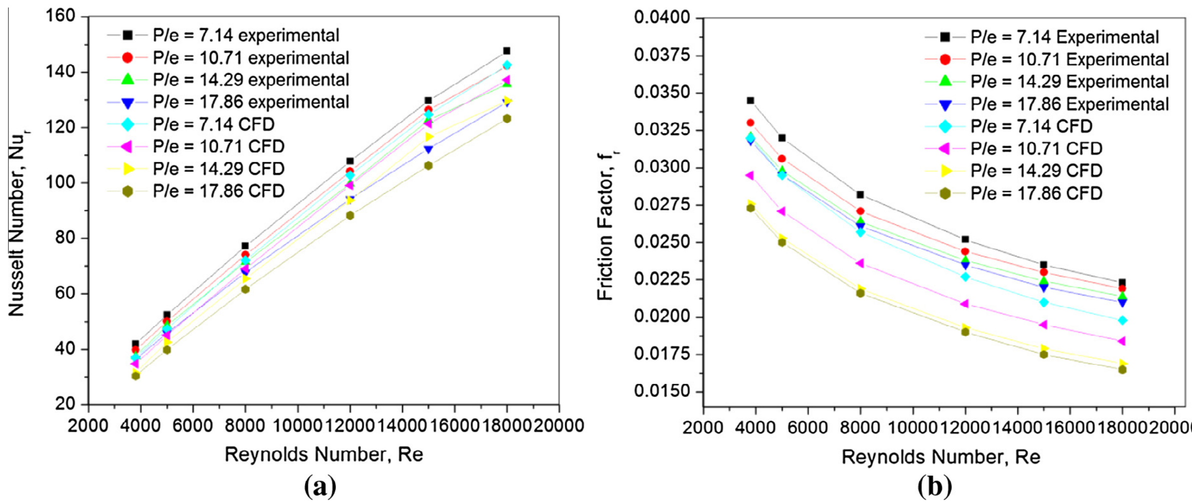

Fig. 21. Comparison of experimentally and numerically (CFD) calculated average (a) Nusselt number and (b) friction factor.

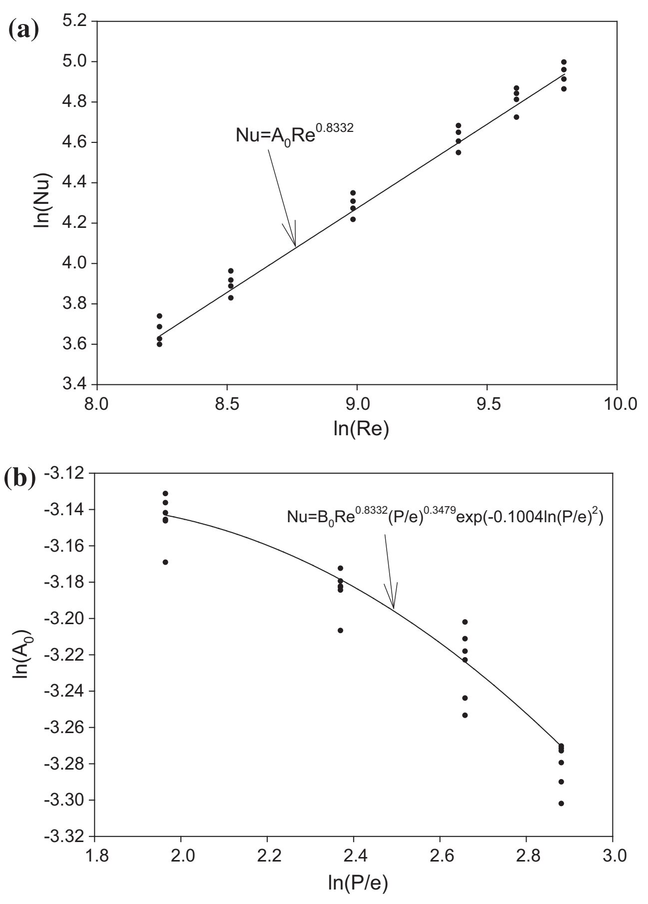

Fig. 22. (a) Plot of Ln (Nu) as a function of Ln (Re) for experimental data and (b) Plot of Ln (A_0) = Ln [$Nu/Re^{0.8332}$] as a function of Ln (P/e).

$$Or \qquad Nu = B_0 Re^{0.8332}(P/e)^{0.3479} \tag{24}$$

The value of coefficient B_0 is a function of relative roughness pitch (P/e). It was observed that second order polynomial equation best described the relationship between Nusselt number and relative roughness pitch.

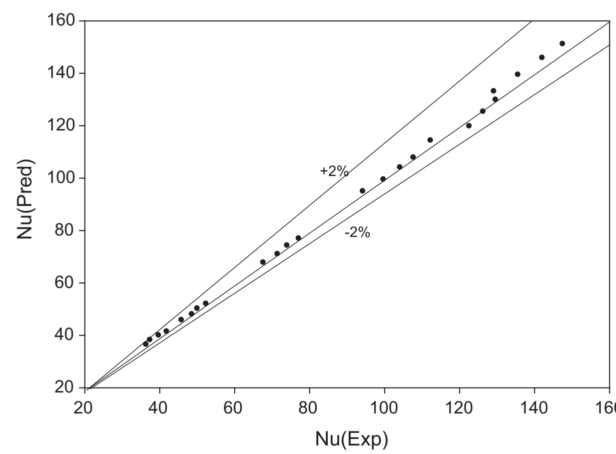

Fig. 23. Comparison of experimental and predicted values of Nusselt number.

The values of A_0 and B_0 are found to be 0.0397 and 0.03209 respectively. The values of Ln (A_0) and Ln (P/e) have been plotted and is shown in Fig. 22(b). Fig. 23 shows the comparison between the Nusselt number obtained from experimental investigations and those predicted by the correlations. It has been observed that about 99% of the predicted data points lie within ±2% deviation lines of the experimental results. The final correlation for Nu can be written as:

$$Nu = 0.032 Re^{0.8332}(P/e)^{0.3479}\exp(-0.1004\ln(P/e)^2) \tag{25}$$

A similar procedure has been adopted to develop a statistical correlation for friction factor on the basis of regression analysis of data obtained from the experimental investigations. The various plots obtained for developing correlation for friction factor are shown in Fig. 24 (a) and (b). The values of A_1 and B_1 are found to be 0.2845 and 0.2805 respectively. The final statistical correlation resulted for friction factor on the basis of regression analysis has the form of,

$$f = 0.2805Re^{-0.2617}(P/e)^{0.0815}\exp(-0.0319\ln(P/e)^2) \quad (26)$$

Fig. 25 shows the comparison between the experimental values of friction factor and those obtained using the correlation. About 99% of the predicted values of the data lie within ±2.5% of the experimentally observed data values. Therefore, the correlations developed for Nusselt number and friction factor are reasonably satisfactory for the prediction of Nusselt number and friction factor of roughened duct in the range of parameters investigated.

6. Conclusions

The experimental and two dimensional CFD analysis of an artificially roughened solar air heater reverse L-shaped rib roughness on the absorber plate has been carried out in the present paper. The effect of relative roughness pitch and Reynolds number on heat transfer enhancement and flow friction characteristics is studied. The main out comings of the experimental investigations are:

(1) The average Nusselt number increases with the increase in Reynolds number. The average Nusselt number increases with the decrease in relative roughness pitch (P/e) at constant relative roughness height (e/D).
(2) The maximum enhancement in Nusselt number has been found to be 2.827 times over the smooth duct corresponding to relative roughness pitch (P/e) of 7.14, relative roughness height (e/D) of 0.042 at Reynolds number (Re) of 15,000 in the range of parameters investigated.
(3) The average friction factor decreases with the increase in Reynolds number. The average values of friction factor increases as the relative roughness pitch decreases for a fixed value of relative roughness height.
(4) The maximum enhancement in the friction factor has been found to be 3.424 times over the smooth duct corresponding to relative roughness pitch (P/e) of 7.14, relative roughness height (e/D) of 0.042 at Reynolds number (Re) of 3800 in the range of parameters investigated.
(5) The value of thermo hydraulic performance parameter which is used for the prediction of optimum reverse L-shaped rib configuration in the system under analysis lies between 1.62 and 1.90 for the range of parameters investigated.
(6) The optimum value of thermo–hydraulic performance parameter for reverse L-shaped rib configuration for the range of parameters investigated in the present system has been found to be 1.90 corresponding to relative roughness pitch (P/e) of 7.14, relative roughness height (e/D) of 0.042 and Reynolds number of 15,000. So, the present model can be employed for heat transfer augmentation.

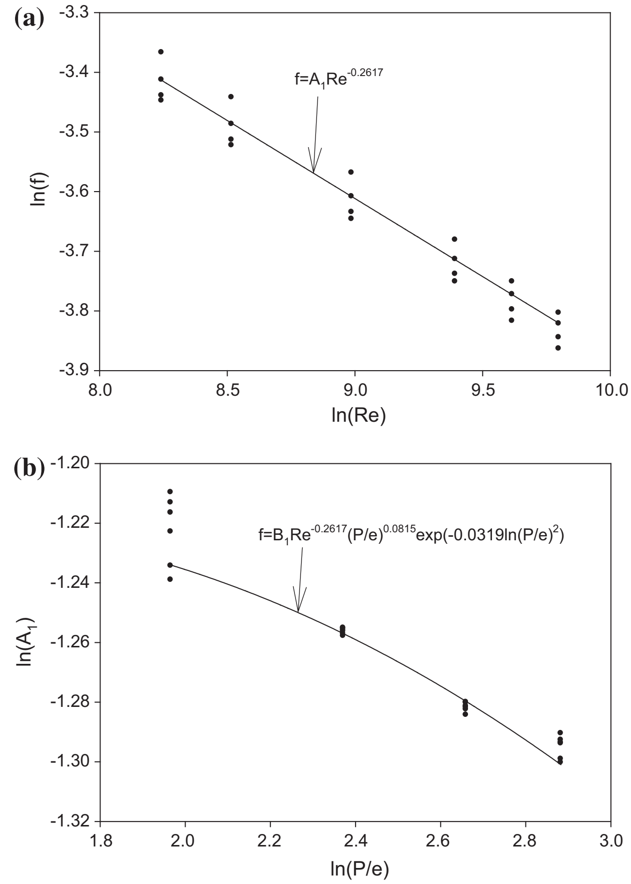

Fig. 24. (a) Plot of Ln (f) as a function of Ln (Re) for experimental data and (b) Plot of Ln (A_1) = Ln [$f/Re^{-0.2617}$] as a function of Ln (P/e).

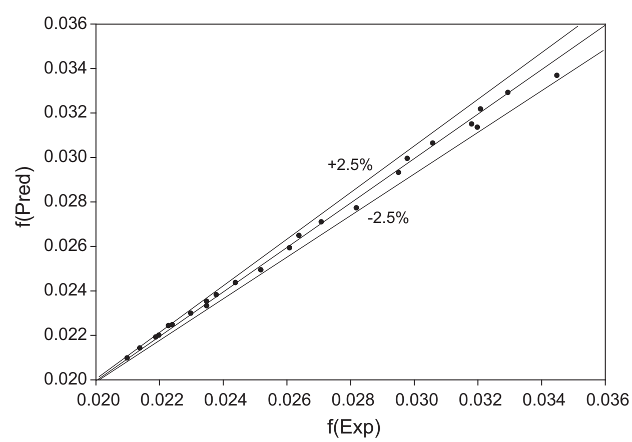

Fig. 25. Comparison of experimental and predicted values of friction factor.

(7) The results of CFD analysis are found to be in good agreement with the experimental results and with the standard theoretical approaches. So the present CFD module can be used for the analysis of the new geometries in solar air heater.

(8) The comparison of experimental values of Nusselt number and friction factor and those predicted by the correlation lie in the deviation range of ± 2 and ± 2.5 respectively. So the present correlations are reasonably satisfactory for the prediction of Nusselt number and friction factor for the roughened duct.

References

Aharwal, K.R., Gandhi, B.K., Saini, J.S., 2008. Experimental investigation on heat-transfer enhancement due to a gap in an inclined continuous rib arrangement in a rectangular duct of solar air heater. Renewable Energy 33, 585–596.

Alam, Taish, Saini, R.P., Saini, J.S., 2014. Use of turbulators for heat transfer augmentation in an air heater duct – a review. Renew. Energy 62, 689–715.

ASHRAE Standard 93, 2003. Method of Testing to Determine the Thermal Performance of Solar Collectors. 30329. American Society of Heating, Refrigeration and Air Conditioning Engineers, Atlanta, GA.

Bhagoria, J.L., Saini, J.S., Solanki, S.C., 2002. Heat transfer coefficient and friction factor correlations for rectangular solar air heater duct having transverse wedge shaped rib roughness on the absorber plate. Renew. Energy 25, 341–369.

Bhushan, B., Singh, R., 2011. Nusselt number and friction factor correlations for solar air heater duct having artificially roughened absorber plate. Sol. Energy 85, 1109–1118.

Bopche, S.B., Tandale, M.S., 2009. Experimental investigation on heat transfer and frictional characteristics of a turbulator roughened solar air heater duct. Int. J. Heat Mass Transfer 52, 2834–2848.

Chaube, A., Sahoo, P.K., Solanki, S.C., 2006. Analysis of heat transfer augmentation and flow characteristics due to rib roughness over absorber plate of a solar air heater. Renewable Energy 31 (3), 317–331.

Fluent, Ansys, 2012. 14.5 Documentation. Ansys, Inc.

Fox, W., Pritchard, P., McDonald, A., 2010. Introduction to Fluid Mechanics. John Wiley & Sons, New York, p. 754.

Gawande, V.B., Dhoble, A.S., Zodpe, D.B., 2014a. Effect of roughness geometries on heat transfer enhancement in solar thermal systems – a review. Renew. Sustain. Energy Rev. 32, 347–378.

Gawande, V.B., Dhoble, A.S., Zodpe, D.B., 2014b. CFD analysis to study effect of circular vortex generator placed in inlet section to investigate heat transfer aspects of solar air heater. Sci. World J. 2014. http://dx.doi.org/10.1155/2014/567257.

Gawande, V.B., Dhoble, A.S., Zodpe, D.B., Chamoli, Sunil, 2016a. A review of CFD methodology used in literature for predicting thermo-hydraulic performance of a roughened solar air heater. Renew. Sustain. Energy Rev. 54, 550–605.

Gawande, V.B., Dhoble, A.S., Zodpe, D.B., Chamoli, Sunil, 2016b. Experimental and CFD-based thermal performance prediction of solar air heater provided with right-angle triangular rib as artificial roughness. J. Brazil. Soc. Mech. Sci. Eng. 38 (2), 551–579.

Gawande, V.B., Dhoble, A.S., Zodpe, D.B., Chamoli, Sunil, 2016c. Experimental and CFD-based thermal performance prediction of solar air heater provided with with chamfered square rib as artificial roughness. J. Brazil. Soc. Mech. Sci. Eng. 38 (2), 643–663.

Gupta, M.K., Kaushik, S.C., 2009. Performance evaluation of solar air heater having expanded metal mesh as artificial roughness on absorber plate. Int. J. Therm. Sci. 48, 1007–1016.

Gupta, D., Solanki, S.C., Saini, J.S., 1993. Heat and fluid flow in rectangular solar air heater ducts having transverse rib roughness on absorber plates. Sol. Energy 51 (1), 31–37.

Gupta, D., Solanki, S.C., Saini, J.S., 1997. Thermo hydraulic performance of solar air heaters with roughened absorber plates. Sol. Energy 61, 33–42.

Han, J.C., Park, C.K., 1989. Augmented heat transfer in rectangular channels of narrow aspect ratios with rib turbulators. Int. J. Heat Mass Transfer 32, 1619–1630.

Karmare, S.V., Tikekar, A.N., 2007. Heat transfer and friction factor correlation for artificially roughened duct with metal grit ribs. Int. J. Heat Mass Transfer 50, 4342–4351.

Karwa, R., 2003. Experimental studies of augmented heat transfer and friction in asymmetrically heated rectangular ducts with ribs on the heated wall in transverse, inclined, v-continuous and v-discrete pattern. Int. Commun. Heat Mass Transfer 30, 241–250.

Kays, W.B., 1966. Convective Heat and Mass Transfer. Mc Graw Hill Book Co., New York, pp. 197–198.

Kline, S.J., McClintock, F.A., 1953. Describing uncertainties in single sample experiments. Mech. Eng. 75, 3–8.

Kumar, A,. Bhagoria, J.L., Sarviya, R.M., 2008. In: International 19th National & 8th ISHMT-ASME Heat and Mass Transfer Conference Heat Transfer Enhancement in Channel of Solar Air Collector by using Discrete w-shaped Artificial Roughened Absorber.

Kumar, S.T., Mittal, V., Thakur, N.S., Kumar, A., 2011. Heat transfer and friction factor correlations for rectangular solar air heater duct having 60° inclined continuous discrete rib arrangement. Br. J. Appl. Sci. Technol. 3, 67–93.

Lanjewar, A., Bhagoria, J.L., Sarviya, R.M., 2011. Experimental study of augmented heat transfer and friction in solar air heater with different orientations of w-rib roughness. Exp. Thermal Fluid Sci. 35, 986–995.

McAdams, W.H., 1942. Heat Transmission. Mc Graw-Hill, New York.

Momin, A.M.E., Saini, J.S., Solanki, S.C., 2002. Heat transfer and friction in solar air heater duct with v-shaped rib roughness on absorber plate. Int. J. Heat Mass Transfer 45, 3383–3396.

Patankar, S.V., 1980. Numerical Heat Transfer and Fluid Flow. Hemisphere, Washington DC.

Prasad, K., Mullick, S.C., 1983. Heat transfer characteristics of a solar air heater used for drying purposes. Appl. Energy 13 (2), 83–93.

Prasad, B.N., Saini, J.S., 1988. Effect of artificial roughness on heat transfer and friction factor in a solar air heater. Sol. Energy 41 (6), 555–560.

Sahu, M.M., Bhagoria, J.L., 2005. Augmentation of heat transfer coefficient by using 90° broken transverse ribs on absorber plate of solar air heater. Renewable Energy 30, 2063–2075.

Saini, S.K., Saini, R.P., 2008. Development of correlations for Nusselt number and friction factor for solar air heater with roughened duct having arc-shaped wire as artificial roughness. Sol. Energy 82, 1118–3110.

Sethi, M., Varun, Thakur, N.S., 2012. Correlations for solar air heater duct with dimpled shape roughness elements on absorber plate. Sol. Energy 86, 2852–2861.

Varun, Saini, R.P., Singal, S.K., 2008. Investigation of thermal performance of solar air heater having roughness elements as a combination of inclined and transverse ribs on the absorber plate. Renew. Energy 33, 1398–1405.

Webb, R.L., Eckert, E.R.G., 1972. Application of rough surface to heat exchanger design. Int. J. Heat Mass Transfer 15 (9), 1647–1658.

Yadav, A.S., Bhagoria, J.L., 2013a. Numerical investigation of flow through an artificially roughened solar air heater. Int. J. Ambient Energy, 1–14.

Yadav, A.S., Bhagoria, J.L., 2013b. A CFD (computational fluid dynamics) based heat transfer and fluid flow analysis of a solar air heater provided with circular transverse wire rib roughness on the absorber plate. Energy 55, 1127–1142.

Yadav, A.S., Bhagoria, J.L., 2014a. A numerical investigation of square sectioned transverse rib roughened solar air heater. Int. J. Therm. Sci. 79, 111–131.

Yadav, A.S., Bhagoria, J.L., 2014b. A CFD based thermo-hydraulic performance analysis of an artificially roughened solar air heater having equilateral triangular sectioned rib roughness on the absorber plate. Int. J. Heat Mass Transfer 70, 1016–1039.

Yeh, H.M., Chou, W.H., 1991. Efficiency of solar air heaters with baffles. Energy 16, 983–987.